The signaling lipid sphingosine 1-phosphate regulates mechanical pain

Authors and Affiliations: Rose Z. Hill[1], Benjamin U. Hoffman[2, 3], Takeshi Morita[1#], Stephanie M. Campos[4‡], Ellen A. Lumpkin[2, 4], Rachel B. Brem[5, 6], Diana M. Bautista[1, 4, 7, 8*]

1. Department of Molecular and Cell Biology, University of California, Berkeley, CA 94720, USA.
2. Department of Physiology & Cellular Biophysics, Columbia University College of Physicians & Surgeons, New York, NY 10032
3. Medical Scientist Training Program, Columbia University, New York, NY 10032
4. Neurobiology Course, Marine Biological Laboratory, Woods Hole, MA
5. Department of Plant and Microbial Biology, University of California, Berkeley, CA 94720, USA.
6. Buck Institute for Research on Aging, Novato, CA 94945, USA.
7. Helen Wills Neuroscience Institute, University of California, Berkeley, CA 94720, USA.
8. Corresponding author

[#] Current Address: Rockefeller University, New York, NY 10065, USA.

[‡] Current Address: Indiana University, Bloomington, IN 47405, USA.

* Correspondence: dbautista@berkeley.edu

Abstract

Somatosensory neurons mediate responses to diverse mechanical stimuli, from innocuous touch to noxious pain. While recent studies have identified distinct populations of A mechanonociceptors (AMs) that are required for mechanical pain, the molecular underpinnings of mechanonociception remain unknown. Here, we show that the bioactive lipid sphingosine 1-phosphate (S1P) and S1P Receptor 3 (S1PR3) are critical regulators of acute mechanonociception. Genetic or pharmacological ablation of S1PR3, or blockade of S1P production, significantly impaired the behavioral response to noxious mechanical stimuli, with no effect on responses to innocuous touch or thermal stimuli. These effects are mediated by fast-conducting A mechanonociceptors, which displayed a significant decrease in mechanosensitivity in S1PR3 mutant mice. We show that S1PR3 signaling tunes mechanonociceptor excitability via modulation of KCNQ2/3 channels. Our findings define a new role for S1PR3 in regulating neuronal excitability and establish the importance of S1P/S1PR3 signaling in the setting of mechanical pain thresholds.

Introduction

Pain is a complex sensation. It serves to protect organisms from harmful stimuli, but can also become chronic and debilitating following tissue injury and disease. Distinct cells and molecules detect noxious thermal and mechanical stimuli. Thermal pain is detected by thermosensitive TRP channels in subsets of nociceptors[1,2], and gentle touch is detected by Piezo2 channels in low-threshold mechanoreceptors (LTMRs)[3,4]. Aδ high-threshold mechanoreceptors (HTMRs) have been shown to play a key role in responses to painful mechanical stimuli[5,6].

Recent studies have shown that there are at least two populations of HTMRs that mediate responses to noxious mechanical stimuli. The *Npy2r*$^{+}$ subpopulation of HTMRs mediates fast paw withdrawal responses to pinprick stimulation and terminates as free nerve endings in the epidermis[5]. The *Calca*$^{+}$ subpopulation of circumferential-HTMRs responds to noxious force and hair pulling, and terminates as circumferential endings wrapped around guard hair follicles[6]. Additionally, somatostatin-expressing interneurons of laminae I-III in the dorsal horn of the spinal cord receive input from nociceptors and are required for

77 behavioral responses to painful mechanical stimuli[7]. Despite these advances in defining the cells and
78 circuits of mechanical pain, little is known about the molecular signaling pathways in mechanonociceptors.
79
80 Here, we show that sphingosine 1-phosphate (S1P) is required for mechanical pain sensation. S1P is a
81 bioactive lipid that signals via 5 G-protein coupled S1P Receptors (S1PRs 1-5). S1P signaling, mainly via
82 S1PR1, plays a well-known role in immune cell migration and maturation[8–10]. Additionally, recent studies
83 have shown that S1PRs are expressed throughout the nervous system[11–13] and S1P signaling is associated
84 with a variety of neuroinflammatory disorders, including multiple sclerosis[14] and Alzheimer's disease[15]. S1P
85 has been implicated in spontaneous pain[13] and thermal pain hypersensitivity[12,16,17], but due to conflicting
86 accounts of S1P receptor expression in the CNS[11,18] and PNS[12,13,19] as well as inconsistent reports on the
87 effects of S1P on neuronal excitability[13,20,21] and pain behaviors[12,13,16,17], the role of S1P in somatosensation
88 remains controversial.
89
90 We found that mice lacking the S1P receptor S1PR3 display striking and selective deficits in behavioral
91 responses to noxious mechanical stimuli. Likewise, peripheral blockade of S1PR3 signaling or S1P
92 production impairs mechanical sensitivity. We show that S1P constitutively enhances the excitability of
93 A mechanonociceptors (AMs) via closure of KCNQ2/3 potassium channels to tune mechanical pain
94 sensitivity. The effects of S1P are completely dependent on S1PR3. While previous studies have shown
95 that elevated S1P triggers acute pain and injury-evoked thermal sensitization[12,13], we now demonstrate that
96 baseline levels of S1P are necessary and sufficient for setting normal mechanical pain thresholds. By
97 contrast, elevated S1P selectively triggers thermal sensitization via activation of TRPV1^{+} heat nociceptors,
98 with no effect on mechanical hypersensitivity. Our findings uncover an essential role for constitutive S1P
99 signaling in mechanical pain.
100

101 Results

102 To identify candidate genes underlying mechanosensation, we previously performed transcriptome
103 analysis of the sensory ganglia innervating the ultra-sensitive tactile organ (the star) of the star-nosed
104 mole[22]. Immunostaining revealed the tactile organ is preferentially innervated by myelinated Aδ fibers[22],

105 which are primarily mechanosensitive. While our original analysis focused on ion channels enriched in the
106 neurons of the star organ, our dataset also revealed enrichment of several components of the S1P
107 pathway, including *S1pr3*. Likewise, single-cell RNA seq of mouse dorsal root ganglion (DRG) neurons
108 revealed *S1pr3* expression in a subset of myelinated mechanoreceptors[19] in addition to a subpopulation of
109 peptidergic C nociceptors.
110
111 S1P promotes excitability in small-diameter, capsaicin-sensitive nociceptors[12,13,20,21]. In addition, S1PR3
112 has been shown to mediate spontaneous pain triggered by elevated S1P and thermal sensitization
113 following sterile tissue injury[13]. However, no studies have examined the role of S1PR3 in
114 mechanosensation or in regulating somatosensory behaviors under normal conditions. Given the
115 enrichment of *S1pr3* in mechanosensory neurons of the star-nosed mole and mouse, we hypothesized that
116 S1P signaling via S1PR3 may also play a role in mechanosensation. Thus, we set out to define the role of
117 S1P signaling and S1PR3 in somatosensory mechanoreceptors.
118
119 **S1PR3 mediates acute mechanical pain**
120 We first examined a variety of somatosensory behaviors in mice lacking S1PR3[23] (*S1pr3*$^{tm1Rlp/Mmnc}$; referred
121 to herein as S1PR3 KO). We initially investigated baseline responses to mechanical stimuli. S1PR3 KO
122 mice displayed a dramatic loss of mechanical sensitivity (**Figure 1A; see Figure 1-source data 1**), as von
123 Frey paw withdrawal thresholds were significantly elevated in S1PR3 KO mice relative to WT and S1PR3
124 HET littermates (mean thresholds: 1.737 g vs. 0.736 and 0.610 g, respectively). Moreover, S1PR3 KO
125 mice demonstrated decreased responses to a range of noxious tactile stimuli (2-6 g; **Figure 1B**) and to
126 noxious pinprick stimulation (**Figure 1C**), but normal responsiveness to innocuous tactile stimuli (0.6-1.4g;
127 **Figure 1B**). S1PR3 KO mice exhibited normal tape removal attempts[3] (**Figure 1D**), righting reflexes
128 (**Figure 1-figure supplement 1A**), radiant heat withdrawal latencies (**Figure 1E**), and itch-evoked
129 scratching (**Figure 1-figure supplement 1B**). These results demonstrate a selective role for S1PR3 in
130 acute mechanical pain.
131
132 As a complement to our analysis of somatosensation in S1PR3 KO animals, we employed a

133 pharmacological approach, using the S1PR3-selective antagonist TY 52156 (TY)[24]. Similar to the
134 phenotype of knockout animals, intradermal injection of 500 μM TY into the mouse hindpaw (the site of
135 testing) triggered a rapid and significant elevation in von Frey paw withdrawal thresholds (**Figure 1F**) and
136 decreased responsiveness to noxious (2-6 g), but not innocuous (0.6-1.4g), tactile stimuli (**Figure 1G**),
137 without affecting noxious heat sensitivity (**Figure 1-figure supplement 1C**). By contrast, blockade of
138 S1PR1 with the selective antagonist W146[16] had no effect on baseline mechanical or thermal thresholds
139 (**Figure 1F; Figure 1-figure supplement 1C**). Overall, these data show that S1PR3 signaling sets
140 mechanical pain sensitivity.
141
142 **Endogenous S1P mediates acute mechanical pain**
143 We next asked whether peripheral S1P was required for the S1PR3-dependent effects on
144 mechanosensation. We decreased S1P levels via injection of the sphingosine kinase inhibitor SKI II to
145 block local production of S1P[25] or elevated S1P levels via intradermal injection of S1P and measured
146 behaviors 30 minutes after injection. Decreasing local S1P levels with SKI II significantly reduced
147 mechanical sensitivity (**Figure 2A; see Figure 2-source data 1**), comparable to the hyposensitivity
148 phenotype observed in S1PR3 KO mice (**Figure 1A**). Again, similar to what was observed in S1PR3 KO
149 animals (**Figure 1E**), peripheral blockade of S1P production had no effect on baseline thermal sensitivity
150 (**Figure 1-figure supplement 1C**). Surprisingly, injecting exogenous S1P (10 μM; maximum solubility in
151 saline vehicle) had no effect on mechanical sensitivity (**Figure 2A-B**). However, as previously reported[12,13],
152 S1P injection triggered S1PR3-dependent thermal hypersensitivity and spontaneous pain (**Figure 2C-D**),
153 demonstrating that the lack of effect on mechanical hypersensitivity is not due to problems with S1P
154 delivery or degradation.
155
156 These data support a model whereby S1P constitutively activates S1PR3 to set normal mechanical pain
157 thresholds. To further test this model, we asked if the mechanical hyposensitivity elicited after endogenous
158 S1P depletion (via SKI II) could be rescued by local injection of exogenous S1P. Indeed, we found that
159 injection of exogenous S1P reversed SKI II-induced mechanical hyposensitivity in a dose-dependent
160 manner, and observed a maximal effect with 200 nM S1P (**Figure 2E**). Although quantification of native

161 S1P levels in skin is inaccurate owing to avid lyase activity[26], our data establish that baseline S1P levels
162 are sufficient to maximally exert their effect on S1PR3-dependent mechanical pain, such that increased
163 S1P does not evoke mechanical hypersensitivity, but diminished S1P leads to mechanical hyposensitivity.
164 These data show that constitutive activation of S1PR3 by S1P is required for normal mechanosensitivity.
165

166 **S1PR3 is expressed in A mechanonociceptors and thermal nociceptors**

167 Our behavioral data showing distinct roles for S1PR3 in mechanonociception and thermal hypersensitivity
168 suggest that S1PR3 is expressed in distinct subsets of somatosensory neurons. While a previous study
169 suggested that all somatosensory neurons express S1PR3[13], single cell RNA seq data suggests *S1pr3* is
170 not expressed by all DRG neurons[19], and no studies have performed quantitative analysis of S1PR3
171 staining or co-staining to define subpopulations of S1PR3^{+} neurons. We thus set out to characterize the
172 somatosensory neuron subtypes expressing *S1pr3* using *in situ* hybridization (ISH) of wild-type
173 somatosensory ganglia and immunohistochemistry (IHC) in an *S1pr3*$^{mCherry/+}$ reporter mouse[27].
174

175 We first used *in situ* hybridization (ISH) with a specific *S1pr3* probe to examine expression patterns of
176 *S1pr3* (**Figure 3A-B**; see **Supplementary File 1**). In our experiments, 43% of cells from wild-type DRG
177 expressed *S1pr3*. Co-ISH revealed that one population of *S1pr3*$^{+}$ neurons represents Aδ
178 mechanonociceptors (AMs). These cells expressed *Scn1a* (39.9% of all *S1pr3*$^{+}$), a gene that encodes the
179 Nav1.1 sodium channel, which mediates mechanical pain in Aδ fibers[28]. *S1pr3*$^{+}$ cells also co-expressed
180 *Npy2r* (20.4% of all *S1pr3*$^{+}$), a marker of a subset of mechanonociceptive A fibers[5]. *S1pr3* was expressed
181 in 70.6% of *Scn1a*$^{+}$ cells and 72% of *Npy2r*$^{+}$ cells, comprising a majority of both of these populations.
182 Interestingly, a subset of cells co-expressed *S1pr3* and the mechanically sensitive channel *Piezo2*, which is
183 expressed by Aβ, Aδ, and C fibers[3]. The remaining *S1pr3*$^{+}$ cells were *Trpv1*$^{+}$ and/or *Trpa1*$^{+}$ C nociceptors
184 (67.1% of all *S1pr3*$^{+}$), which are reported to overlap minimally with the *Scn1a*$^{+}$ and *Npy2r*$^{+}$ populations[5,28].
185

186 We next used an *S1pr3*$^{mCherry/+}$ reporter mouse, which produces a functional S1PR3-mCherry fusion
187 protein[27], as an independent strategy to explore S1PR3 expression and localization. This strategy was
188 used because we found that anti-S1PR3 antibodies showed broad immunoreactivity in DRG from mice
189 lacking S1PR3, and so we instead used anti-DsRed antibodies to probe expression of the S1PR3 fusion

190 protein (**Figure 3-figure supplement 1E**). We found that 42.4% S1PR3$^+$ cells co-stained with anti-
191 Peripherin, demonstrating that S1PR3 is expressed in a subset of small-diameter neurons. We also
192 observed that 69.5% of S1PR3$^+$ cells co-stained with anti-NF200, which marks medium and large-diameter
193 myelinated neurons. Furthermore, we observed that S1PR3$^+$ cells were primarily of small to medium
194 diameter (11.3-35.1 μm), whereas all cells in the DRG ranged from 11.3-53.9 μm. Overall, these data
195 support the expression of S1PR3 in subsets of small-diameter thermal nociceptors and medium-diameter
196 mechanonociceptors (**Figure 3F**). Additionally, no significant differences were observed between WT and
197 S1PR3 KO DRG in number of *Trpa1, Trpv1,* Peripherin-, NF200-, or IB4-positive cells (**Figure 3-figure**
198 **supplement 1B-C, F, G**). The mean diameters of *Trpv1*$^+$ neurons (**Figure 3-figure supplement 1D**, left),
199 NF200$^+$ neurons (**Figure 3-figure supplement 1G**), or all neurons (**Figure 3-figure supplement 1D**, right)
200 in WT versus KO DRG were not significantly different, suggesting no loss of major sensory neuronal
201 subtypes in the S1PR3 KO.
202
203 We then visualized S1PR3 expression in nerve fibers that innervate the skin using anti-DsRed antibodies in
204 whole-mount immunohistochemistry (IHC; **Figure 3D**). The reporter animals showed no specific antibody
205 staining in epidermal or dermal cells (**Figure 3-figure supplement 1I**), and single-cell RNA seq of a
206 diverse array of mouse epidermal and dermal cells corroborates this lack of expression[29]. We observed
207 overlap of S1PR3-expressing free nerve endings with NF200-positive myelinated free nerves and NF200-
208 negative putative C-fiber endings (**Figure 3F**), but did not observe expression of S1PR3 in NF200-positive
209 circumferential or lanceolate hair follicle receptors, or in putative Merkel afferents (**Figure 3D-E**). β-tubulin
210 III, PGP9.5 (pan-neuronal markers), and NF200 staining in S1PR3 KO skin displayed patterns of epidermal
211 and dermal innervation similar to WT skin, suggesting the phenotypes observed in the S1PR3 KO mice are
212 not due to developmental loss of sensory neuronal innervation ($p_{PGP9.5}$ = 0.443 (n = 93, 38 fibers); p_{NefH} =
213 0.405 (n = 61, 28 fibers); p_{BTIII} = 0.353 (n = 104, 89 fibers); two-tailed t-tests based on average number of
214 fibers per field of view). These results support expression of S1PR3 in subsets of myelinated A
215 mechanonociceptors and unmyelinated C nociceptors that terminate as free nerve endings.
216
217

218 **S1P activates thermal nociceptors but not putative AMs**

219 Live imaging of cultured DRG neurons from adult reporter animals showed expression of S1PR3-mCherry
220 fusion protein in 48.3% of neurons, mirroring our ISH and IHC results (**Figure 4A**). To examine the effects
221 of S1P on A mechanonociceptors and C nociceptors, we performed ratiometric calcium imaging and
222 electrophysiology on DRG cultures from reporter mice. Interestingly, only 56.1 ± 22.4 % of mCherry-
223 expressing neurons were activated by 1 μM S1P (Representative trace in **Figure 4B**; representative
224 images in **Figure 4C**), which our dose-response showed to be the saturating concentration for calcium
225 influx (**Figure 4D**; EC_{50} = 155 nM). All S1P-responsive neurons were also capsaicin-sensitive (n > 2000
226 neurons). And while sensory neurons from S1PR3 KO animals did not respond to S1P, as expected[13], they
227 exhibited capsaicin responses that were not significantly different from WT neurons (**Figure 3-figure**
228 **supplement 1H**). The mean diameter of S1P-responsive $mCherry^+$ neurons was 22.4 ± 1.0 μm, whereas
229 the mean diameter of non-responsive $mCherry^+$ neurons was 28.7 ± 3.2 μm (p = 0.0002, two-tailed t-test).
230 We also performed whole cell current clamp experiments and, consistent with other studies[12,20,21], found
231 that S1P evoked action potential firing in capsaicin-sensitive small diameter cells (**Figure 4E**). This shows
232 that only the small-diameter, $S1PR3^+$ putative nociceptors are excited by S1P. We next asked whether the
233 $S1PR3^+$ medium-large diameter neurons represent the mechanonociceptors observed by ISH (**Figure 3A**).
234 To this end, we asked whether the spider toxin Hm1a, a selective activator of AM nociceptors[28], triggers
235 calcium influx in S1PR3-expressing trigeminal neurons. Indeed, we found that 44.2 ± 15.1% of Hm1a-
236 responsive neurons expressed mCherry (**Figure 4F**), consistent with our staining showing expression of
237 *S1pr3* in AM nociceptors and the role of Hm1a-responsive neurons in mediating mechanical pain *in vivo*[28].

238

239 **S1PR3 modulates KCNQ2/3 channels to regulate AM excitability**

240 We next interrogated the molecular mechanism by which S1P signaling in AM nociceptors may regulate
241 mechanical pain. We performed whole-cell current clamp on the medium-diameter $S1pr3^{mCherry/+}$ dissociated
242 DRG neurons (membrane capacitance = 61.05 ± 1.92 pF), which did not display S1P-evoked calcium influx
243 (**Figure 4B-C**). In these cells, 1 μM S1P application did not change membrane potential (**Figure 5-figure**
244 **supplement 1A;** see **Figure 5-source data 1**) or elicit firing in the absence of current injection (**Figure 5-**
245 **figure supplement 1A**; **Figure 5A**). However, S1P dramatically lowered the threshold to fire action

246 potentials (rheobase) in an S1PR3-dependent manner (**Figure 5A**, **Figure 5-figure supplement 1B**).

247

248 We then set out to determine the mechanism by which S1PR3 activity increases neuronal excitability using
249 whole-cell voltage clamp recording. Previous studies showed that S1P excites capsaicin-sensitive
250 nociceptors by increasing voltage-gated sodium currents and reducing steady-state potassium currents[20,21].
251 We found that S1P had no such effects on S1PR3^{+} medium-diameter cells (**Figure 5-figure supplement**
252 **1C-E**). By contrast, S1P triggered a robust increase in input resistance (**Figure 5B**), consistent with the
253 closure of potassium channels. I-V analysis revealed that the current inhibited by S1P application was
254 carried by potassium (**Figure 5C**). Additionally, S1P significantly reduced slow, voltage-dependent tail
255 current amplitudes (**Figure 5-figure supplement 1F**; **Figure 5D** (top)) in an S1PR3-dependent manner
256 (**Figure 5-figure supplement 1F**, center).

257

258 As tail currents in Aδ neurons are primarily mediated by KCNQ2/3 potassium channels[30,31], we postulated
259 that S1P may alter tail currents through modulation of these channels. Furthermore, the above properties
260 of the S1P-sensitive current were consistent with the reported electrophysiological properties of KCNQ2/3
261 channels in DRG neurons[30,32,33]. To address whether KCNQ2/3 channels mediated S1P-dependent
262 neuronal excitability, we applied the KCNQ2/3-selective inhibitor XE 991 and found that it completely
263 occluded the effects of S1P on tail current (**Figure 5D**). Similar results were observed with the related
264 antagonist, linopirdine (**Figure 5D**). These findings are consistent with S1P/S1PR3-dependent inhibition of
265 KCNQ2/3 in somatosensory neurons.

266

267 We also found that the effect of S1P on KCNQ2/3 currents was mediated by low levels of S1P, exhibiting
268 an IC_{50} of 48 nM with saturation at 100 nM (**Figure 5-figure supplement 1G**). While S1P cannot be
269 accurately measured in non-plasma tissues, this is similar to estimated levels of S1P in peripheral
270 tissues[10,34], and to levels which rescued mechanosensitivity after local S1P depletion (**Figure 2E**). Thus,
271 our *in vitro* IC_{50} supports our behavioral observations that baseline S1P levels are sufficient to maximally
272 exert their effect on mechanical pain. In summary, our electrophysiological and behavioral observations
273 support a model in which baseline S1P/S1PR3 signaling governs mechanical pain thresholds through

modulation of KCNQ2/3 channel activity in AM neurons (**Figure 8**).

S1PR3 is required for nociceptive responses of high-threshold AM nociceptors

Given the effects of S1P on putative AM neurons *in vitro* and the selective attenuation of baseline mechanical pain in S1PR3 KO animals, we hypothesized that S1PR3 would play a role in AM afferent function. To test this, we utilized *ex vivo* skin-nerve recordings to analyze the effects of genetic ablation of S1PR3 on AM afferents, which mediate fast mechanical pain sensation. S1PR3 HET animals were used as littermate controls because no significant differences were observed between S1PR3 WT and S1PR3 HET mice in any behavioral assay (**Figure 1**), and because force-response relationships are comparable between S1PR3 HET AM fibers and wild type AM recordings[28,35–38] (**Figure 6-figure supplement 1A;** see **Figure 6-source data 1**). Compared to S1PR3 HET, S1PR3 KO AM nociceptors displayed reduced sensitivity in their force-response relation (slope for HET versus KO: 50 Hz/N versus 35 Hz/N), as well as attenuated firing over the noxious, but not innocuous, range of mechanical stimulation (**Figure 6A**). Strikingly, the median von Frey threshold to elicit firing in AM nociceptors was significantly higher in S1PR3 KO animals (3.92 mN) compared to littermate controls (1.56 mN; **Figure 6B**). Furthermore, S1PR3 KO AM nociceptors displayed a right-shifted cumulative response curve to force-controlled stimuli (50% effective force for HET versus KO: 33.7 versus 60.0 mN; **Figure 6C**), consistent with the mechanonociceptive hyposensitivity observed *in vivo*. By contrast, neither AM conduction velocities nor the conduction velocity distributions of Aβ, Aδ, and C fibers differed between genotypes (**Figure 6D** and **Figure 6-figure supplement 1B**).

A recent study reported that A-nociceptors are composed of two genetically distinct neuronal populations that differ in conduction velocity and in adaptation properties[5] ("Adapting AM" versus "Non-adapting AM"). We next asked whether loss of S1PR3 signaling altered these AM subtypes. Adapting AM fibers responded more vigorously to dynamic (ramp) stimuli than to static (hold) stimuli, and displayed a mean dynamic firing frequency at least twofold greater than their static firing frequency[5] (**Figure 6E, upper traces**). By contrast, Non-adapting AM fibers often showed bursting during static stimulation, which resulted in similar firing rates during dynamic and static stimulation (**Figure 6E, lower traces**). S1PR3 KO

302 animals displayed a significantly lower proportion of Adapting AM nociceptors compared with littermate
303 controls (**Figure 6F**). Additionally, we observed an increase in S1PR3 KO AM fibers that were
304 unresponsive to controlled force stimulation (**Figure 6F**). These "non-responders" only fired action
305 potentials to high-pressure stimuli with a blunt glass probe or to suprathreshold stimulation with von Frey
306 filaments (see Methods). The Non-adapting AMs, and the few remaining mechanosensitive Adapting AMs
307 in the S1PR3 KO displayed similar firing frequencies over both the dynamic and static phases of force
308 application to control fibers (**Figure 6-figure supplement 1C**). This suggests that decreased
309 mechanosensitivity of the Adapting AM population accounts for the significant reduction in force-firing
310 relations observed at the population level in S1PR3 KO AMs (**Figure 6A**). We conclude that S1PR3 is an
311 essential regulator of both mechanical threshold and sensitivity in a distinct population of AM nociceptors.
312

313 **S1PR3 is required for inflammatory pain hypersensitivity**

314 Having examined the mechanisms of S1P/S1PR3 signaling in acute mechanonociception, we next sought
315 to evaluate S1P/S1PR3 signaling in pain hypersensitivity. For this purpose, we used an experimental
316 model of inflammatory pain triggered by Complete Freund's Adjuvant (CFA) injection into the hindpaw,
317 which elicits infiltration of immune cells and thermal and mechanical hypersensitivity[39]. While one previous
318 study proposed that S1PR3 promotes injury-evoked heat and mechanical hypersensitivity, they did not
319 measure or compare post-injury mechanical thresholds to pre-injury baselines for the knockout or control
320 animals[13]. Here, we compared development of CFA-evoked hypersensitivity between S1PR3 HET and KO
321 littermates, since no significant behavioral differences were observed between WT and HET animals in
322 CFA experiments ($p_{\text{von Frey}} = 0.12$; $p_{\text{radiant heat}} = 0.12$; two-tailed *t*-tests). Strikingly, S1PR3 KO mice failed to
323 develop thermal hypersensitivity (**Figure 7A;** see **Figure 7-source data 1**) relative to heterozygous
324 littermates at both 24 and 48 hours post-CFA injection. In stark contrast, S1PR3 KO animals developed
325 robust mechanical hypersensitivity when thresholds were normalized to account for the dramatic baseline
326 differences between knockouts and control animals (**Figure 7B**). Our data demonstrate that S1PR3
327 mediates baseline mechanical sensitivity and is not required for the development of CFA-evoked
328 mechanical hypersensitivity.
329

330 Influx of myeloid lineage ($Cd11b^+/Ly6G^-$) cells is required for the development of mechanical
331 hypersensitivity in the CFA model[39]. In the immune system, S1P signaling via S1PR1 plays a key role in
332 immune cell migration[9]. Consistent with the development of mechanical hypersensitivity, flow cytometry
333 experiments showed robust infiltration of immune cells into hindpaw skin from both S1PR3 KO and
334 littermate controls (**Figure 7-figure supplement 1A-B**). These data suggest that the phenotypes observed
335 in S1PR3 KO mice cannot be attributed to compromised immune cell infiltration.
336
337 Next, we tested whether active S1P/S1PR3 signaling was required to maintain CFA-evoked thermal
338 hypersensitivity using pharmacology. Acute blockade of S1P production with SKI II or S1PR3 with TY also
339 reversed CFA heat hypersensitivity (**Figure 7C**), demonstrating that peripheral S1P actively signals via
340 S1PR3 to promote CFA-evoked heat hypersensitivity. Furthermore, acute S1P/S1PR3 blockade with SKI II
341 or TY elevated mechanical thresholds to pre-CFA, baseline levels (**Figure 7D**) showing that S1PR3 tunes
342 mechanical pain under normal and inflammatory conditions. These results are consistent with the distinct
343 roles for AM and C nociceptors in mechanical pain. Under normal conditions, AM nociceptors set
344 mechanical pain thresholds[28,40]. By contrast, under inflammatory conditions, the combined activity of both
345 non-sensitized AM fibers and sensitized C fibers determines overall post-inflammatory mechanical
346 thresholds[41,40]. Consistent with this model, acute blockade of S1P production or S1PR3 activity under
347 normal conditions induces mechanical hyposensitivity and under inflammatory conditions returns
348 mechanical sensitivity to normal levels.
349

350 Discussion

351 We now show that S1P signaling via S1PR3 is a key pathway that tunes mechanical pain sensitivity.
352 Overall, our data reveal two new key findings. First, S1P/S1PR3 sets baseline mechanical pain thresholds.
353 Depletion of baseline, endogenous S1P induces mechanical hyposensitivity and nanomolar levels of
354 exogenous S1P are sufficient to restore normal mechanical pain sensitivity after depletion. Second,
355 elevated micromolar S1P levels, such as those produced during inflammation or disease, promote thermal,
356 but not mechanical hypersensitivity. The effects of S1P on acute mechanical pain and thermal

357 hypersensitivity are completely lost in S1PR3 knockout animals, which are otherwise normal with respect to
358 other somatosensory behaviors.
359
360 What is the local source of S1P in the skin that constitutively modulates mechanical pain? Even in the
361 mature field of S1P signaling in the vascular and immune systems, the cellular source of S1P, while an
362 intriguing question, remains unclear. All cells in the body, including somatosensory neurons, immune cells,
363 and skin cells, express sphingosine kinases 1 and 2 which are essential for S1P production[42]. Deletion of
364 both kinases is lethal and attempts to conditionally knockout these kinases fail to completely eliminate S1P
365 in tissues[43]. While RNA seq data suggests that somatosensory neurons contain all of the enzymatic
366 machinery required to produce and export local S1P[19,44], future work will be needed to identify the key cell
367 types that are important for maintaining baseline S1P levels in the skin to regulate mechanical sensitivity
368 and for increasing S1P under inflammatory/injury conditions to promote pain hypersensitivity.
369
370 Recent studies have identified distinct populations of AM nociceptors that are required for mechanical
371 pain[5,6]. Likewise, it was discovered that a subset of somatostatin-expressing spinal interneurons is required
372 for mechanical pain transduction[7]. Although these papers delineate the cells and circuitry of mechanical
373 pain, the molecular underpinnings of mechanonociception in the periphery are poorly understood. While
374 the identity of the transduction channel(s) in AM nociceptors remains enigmatic, understanding molecular
375 mechanisms that regulate excitability will no doubt provide key insights into the function and specialization
376 of the diverse subtypes of mechanosensitive nerve fibers. For example, although *Piezo2*-hypomorphic
377 animals exhibit normal mechanical pain behaviors[3], *ex vivo* skin-nerve recordings show that their AM
378 nociceptors display decreased force-responsiveness[3], and a recent study found that subpopulations of
379 sensory neurons express different splice variants of *Piezo2* that exhibit different force sensitivities[45]. These
380 studies suggest that mechanosensitive neurons exhibit functional specialization on multiple levels. Our
381 study demonstrates that S1PR3 is indispensable for normal function of AM nociceptors, including the
382 adapting AM population, recently discussed in Arcourt *et al.,* that innervates the epidermis and encodes
383 noxious touch[5]. We show that S1PR3 signaling modulates KCNQ2/3 channels to regulate excitability of
384 these A mechanonociceptors (**Figure 8**).

385

386 GPCR-mediated inhibition of KCNQ2/3 potassium channels is a well-known mechanism by which neuronal
387 excitability is regulated[46]. Other studies have shown that KCNQ channels mediate excitability of Aδ
388 fibers[30,31] and are required for normal mechanonociceptive responses in dorsal horn neurons receiving Aδ
389 input[31], and that opening KCNQ2/3 channels directly with retigabine alleviates pain *in vivo*[33,47,48]. Our
390 results not only complement previous work implicating KCNQ2/3 channels in pain, but also define the
391 upstream mechanisms that promote the regulation of KCNQ2/3 channels to tune mechanical pain
392 thresholds. Our data thus highlight S1PR3 as a novel and attractive target for the treatment of mechanical
393 pain and describe a new signaling pathway by which S1P regulates AM nociceptor excitability.

394

395 Interestingly, the neurons that innervate the ultra-sensitive tactile organ of the star-nosed mole are highly
396 enriched in transcripts for S1PR3 and KCNQ channels, as well as for a variety of other potassium
397 channels[22]. While it is difficult to directly examine the physiological basis for heightened mechanosensitivity
398 in the star-nosed mole, S1PR3-dependent modulation of KCNQ may represent an important mechanism
399 underlying the high tactile sensitivity of the star organ. Moreover, link between *S1pr3* and *Kcnq2/3* are
400 echoed in single-cell RNA seq datasets from mouse DRG neurons, which show co-expression of *S1pr3*
401 and *Kcnq2/3* in a subset of myelinated mechanoreceptors[19]. These cells are distinct from the *S1pr3/Trpv1*
402 subset that mediates S1P-evoked acute pain and heat hypersensitivity. In addition to being transcriptionally
403 distinct, we show that the mechanisms underlying S1P's activities in these cells are functionally distinct.
404 Finally, *S1pr3* and *Kcnq2/3* are highly expressed in human sensory ganglia[49,50] and recordings from human
405 stem cell-derived sensory neurons show that KCNQ2/3 channels play a key role in mediating their
406 excitability[51]. Thus S1PR3 signaling may represent a new target for modulating mechanical pain.

407

408 Previous studies of S1P signaling in DRG neurons focused on S1P-evoked excitation of small diameter
409 and/or capsaicin-sensitive neurons, and pain behaviors triggered by elevated S1P. While our new data
410 affirms the effects S1P in thermal nociceptors observed by others, our manuscript highlights a novel effect
411 of baseline levels of S1P in modulation of rheobase and KCNQ2/3 currents in mechanonociceptors. We
412 are also the first to examine the role of S1PR3 in a variety of somatosensory behaviors under normal

413 conditions (non-injury, no algogen injection), and to demonstrate a key role for S1PR3 in
414 mechanonociception. We also go beyond previous studies[12,13,16,17] in showing that elevated S1P
415 selectively promotes thermal and not mechanical hypersensitivity. Previous studies have shown that there
416 are distinct cells and molecular pathways that trigger thermal versus mechanical hypersensitivity. For
417 example, thermal hypersensitivity in CFA is dependent on TRPV1 ion channels[1] and independent of
418 immune cell infiltration[39]. By contrast, infiltration of a subset of myeloid immune cells is required for
419 mechanical hypersensitivity in an inflammatory pain model[39]. Here we show that S1P via S1PR3 signaling
420 is a key component of the inflammatory soup that triggers thermal hypersensitivity in the CFA model. Our
421 observation that S1PR3 KO animals display normal immune cell infiltration and develop mechanical
422 hypersensitivity after CFA is consistent with these previous studies showing distinct mechanisms of
423 inflammatory thermal and mechanical hypersensitivity.
424
425 Outside of the nervous system, S1P signaling via S1PR1 allows for the continuous circulation of
426 lymphocytes between blood, lymph, and peripheral tissues[9]. Our findings that S1P plays a key role in
427 noxious mechanosensation are in line with recent studies showing that sensory neurons co-opt classical
428 immune pathways to drive chronic itch or pain[52,53]. What distinguishes this study from the others is that S1P
429 signaling is critical for acute mechanical pain, even in the absence of inflammation or exogenously elevated
430 S1P. In the immune system, disruptions in S1P levels or S1PR1 signaling result in significant immune
431 dysfunction and disease[54–56]. Accordingly, in the somatosensory system, excessive, high levels of S1P
432 (micromolar), such as those present in inflammation, evokes thermal pain and sensitization. Intermediate,
433 baseline levels (nanomolar) regulate AM excitability and are required for normal mechanical pain
434 sensation. By contrast, lowering S1P levels reduces mechanical pain sensation, while sparing innocuous
435 touch sensation.
436
437 We propose that S1PR3 signaling may contribute to a variety of inflammatory diseases. S1P has been
438 linked to a wide range of human inflammatory disorders[57–63]. Canonically, S1P signaling via S1PR1 is
439 thought to promote inflammation via the immune system[58], however, we propose that S1P signaling via
440 S1PR3 in neurons may also contribute to inflammatory disease. Indeed, fingolimod, a non-selective S1PR

441 modulator, is prescribed as an immunosuppressant for multiple sclerosis treatment[14], but the possibility that
442 some of its therapeutic effects may also be mediated via the nervous system has not been fully explored.
443 Likewise, one study found that intrathecal fingolimod reduces bone cancer pain[64], and while analgesia was
444 attributed to effects on S1PR1 in glia, some of the benefits may be due to S1PR3 signaling in DRG
445 neurons. S1PR3 antagonism may also be useful in the treatment of inflammatory pain due to its selective
446 dampening of acute mechanical pain and inflammatory thermal hypersensitivity, while preserving
447 innocuous touch and normal thermal sensitivity. S1PR3 inhibitors may also be beneficial for treating other
448 inflammatory disorders where S1PR3-expressing somatosensory neurons have been shown to contribute
449 to neurogenic inflammation, such as asthma[65]. Our study demonstrates a crucial role for S1P signaling in
450 the peripheral nervous system and highlights the potential of S1PR3 as a target for future pain therapies.
451

452 Materials and Methods

453 *Behavioral studies & mice*

454 *S1pr3*$^{mcherry/+}$ and *S1pr3*$^{-/-}$ mice were obtained from Jackson Laboratory and backcrossed to C57bl6/J.
455 Wherever possible, wild-type/heterozygous (*S1pr3)* littermate controls were used in behavioral
456 experiments. Mice (20–25 g) were housed in 12 h light-dark cycle at 21°C. Mice were singly housed one
457 week prior to all behavioral experiments and were between 8-10 weeks at the time of the experiment. All
458 mice were acclimated in behavioral chambers (IITC Life Sciences) on 2 subsequent days for 1 hour prior to
459 all behavioral experiments.
460

461 Itch and acute pain behavioral measurements were performed as previously described[44,66,67]. Mice were
462 shaved one week prior to itch behavior. Compounds injected: 500 μM TY 52156 (Tocris), 50 μM SKI II
463 (Tocris), 0.2-10 μM S1P (Tocris, Avanti Polar Lipids), 50 mM chloroquine (Sigma), and 27 mM histamine
464 (Tocris) in PBS with either 0.01-0.1% Methanol- (S1P) or 0.1-0.5% DMSO-PBS (all other compounds)
465 vehicle controls. Pruritogens were injected using the cheek model (20 μL) of itch, as previously described[68].
466 Behavioral scoring was performed while blind to experimental condition and mouse genotype. All
467 scratching and wiping behavior videos were recorded for 1 hour. Itch behavior was scored for the first 30
468 minutes and acute pain was scored for the first five minutes. Bout number and length were recorded.

469

470 For radiant heat and von Frey hypersensitivity behavior, drugs were injected intradermally into the plantar
471 surface of the hindpaw (20 μL). Radiant heat assays were performed using the IITC Life Science
472 Hargreaves test system. Mechanical threshold was measured using calibrated von Frey monofilaments
473 (Touch Test) on a metal grate platform (IITC). Von Frey was performed as previously described[67,69] using
474 the up-down method[70] while blinded to compound injected and genotype, or a descending force-series of 4
475 trials per force from 0.4 g to 6 g. Valid responses for both von Frey and radiant heat included fast paw
476 withdrawal, licking/biting/shaking of the affected paw, or flinching. For radiant heat and von Frey, mice were
477 allowed to acclimate on platform for 1 hour before injection. Measurements were taken 15 minutes pre-
478 injection and 20-30 minutes post-injection for all compounds used.

479

480 The pinprick assay[7] was conducted on a von Frey testing platform (IITC). The mouse hindpaw was poked
481 with a 31 g syringe needle without breaking the skin to induce fast acute mechanical pain. Each paw was
482 stimulated 10 times with the needle, with five minutes rest in between trials, and the % withdrawal (fast
483 withdrawal, licking/biting/shaking of paw, squeaking, and/or flinching) was calculated from the total number
484 of trials.

485

486 The tape assay was conducted according to previously described methods[3]. Number of attempts to remove
487 a 3 cm piece of lab tape was recorded for 10 minutes after manual tape application to the rostral back.
488 Scorer and experimenter were blinded to genotype.

489

490 For righting reflex measurements, age-matched *S1pr3*$^{-/-}$ and $^{+/+}$ P6-7 neonates were used. Briefly, pups
491 were overturned one at a time on the home cage lid while experimenter was blinded to genotype. The time
492 to righting was measured to the nearest 1/10th of a second with a stopwatch.

493

494 For the CFA model of hypersensitivity, mice were lightly anesthetized with isoflurane (2%) and injected with
495 15 μL CFA (Sigma) into one hindpaw using a Hamilton syringe (30 g) at 5pm. Radiant heat latencies and
496 von Frey 50% withdrawal thresholds were recorded one day prior to CFA, the morning of CFA (prior to

injection), and one and two days post-CFA. Von Frey measurements were acquired before radiant heat latencies, and mice were allowed a one-hour recovery period in home cage with access to food and water in between testing. Both ipsilateral and contralateral paw were measured. Experimenter was blind to genotype for injections and recording.

All behavior experiments were carried out using age-matched or littermate cohorts of male mice and conducted between 8am and 1pm. Mice were tested in 4-part behavior chambers (IITC Life Sciences) with opaque dividers (TAP Plastics) with the exception of righting reflex measurements. Scratching and wiping behaviors were filmed from below using high-definition cameras. All experiments were performed under the policies and recommendations of the International Association for the Study of Pain and approved by the University of California, Berkeley Animal Care and Use Committee.

In situ hybridization (ISH)

Fresh DRG were dissected from 8-12 week old mice, flash frozen in OCT embedding medium, and sectioned at 14 µm onto slides. ISH was performed using Affymetrix Quantigene ViewISH Tissue 2-plex kit according to manufacturer's instructions with Type 1 (*S1pr3*) and Type 6 (all other) probes. The following probes against mouse mRNAs were created by Affymetrix and used for ISH: *S1pr3, Scn1a, Npy2r, Piezo2, Trpv1, Trpa1.*

Immunohistochemistry (IHC) of DRG

DRG were dissected from 8-12 week old adult mice and post-fixed in 4% PFA for one hour. DRG were cryo-protected overnight at 4°C in 30% sucrose-PBS, embedded in OCT, and then cryosectioned at 12 µm onto slides. Briefly, slides were washed 3x in PBST (0.3% Triton X-100), blocked in 2.5% horse serum + 2.5% BSA PBST, and incubated overnight at 4°C in 1:1000 primary antibody in PBST + 0.5% horse serum + 0.5% BSA. Slides were washed 3X in PBS then incubated 1-2 hours at RT in 1:1000 secondary antibody. Slides were washed 3X in PBS and mounted in Fluoromount-G + DAPI with No. 1.5 coverglass. Primary antibodies used: Rabbit anti-DsRed (Clontech #632496), Rabbit anti-S1PR3 (Abcam #38324; #108370), Mouse anti-NF200 (Sigma #N5389), Chicken anti-Peripherin (Abcam #39374). Secondary antibodies used:

525 Goat anti-Mouse Alexa 488 (Abcam #150117), Goat anti-Chicken Alexa 488 (ThermoFisher #A11039),
526 Goat anti-Rabbit Alexa 594 (Invitrogen #R37117). Isolectin B4 (IB4)-FITC (Enzo Life Sciences #ALX-650-
527 001F-MC05) was also used. Slides were mounted in Fluoromount with No. 1.5 coverglass. Imaging of DRG
528 ISH and IHC experiments, and all live-cell imaging, was performed on an Olympus IX71 microscope with a
529 Lambda LS-xl light source (Sutter Instruments). For DRG ISH and IHC analysis, images were analyzed
530 using FIJI software. Briefly, DAPI-positive cells were circled and their fluorescence intensity (AFU) for all
531 channels was plotted against cell size using Microsoft Excel software. Co-labeling analysis was performed
532 using FIJI. Intensity thresholds were set based on the negative control (no probe) slide. Cells were defined
533 as co-expressing if their maximum intensities exceeded the threshold for both channels of interest.
534
535 *IHC of sectioned skin*
536 Skin was dissected from 8 week old adult mice and post-fixed in 4% PFA for 30 minutes at RT. DRG were
537 cryo-protected overnight at 4°C in 30% sucrose-PBS, embedded in OCT, and then sectioned at 18 µm onto
538 slides. Briefly, slides were blocked in 5% normal goat serum in PBST (0.1% Triton X-100) and incubated
539 overnight at 4°C in 1:1000 primary antibody in blocking buffer. Slides were washed 3X in PBS then
540 incubated 45 minutes at RT in 1:1000 secondary antibody. Slides were washed 5X in PBS and mounted in
541 Fluoromount-G + DAPI with No. 1.5 coverglass. Primary antibodies used: Rabbit anti-DsRed (Clontech
542 #632496), Chicken anti-NefH (Abcam #4680), Chicken anti-β-tubulin III (Abcam #107216), mouse anti-
543 PGP9.5 (Abcam #8189). Secondary antibodies used: Goat anti-Mouse Alexa 488 (Abcam #150117), Goat
544 anti-Rabbit Alexa 594 (Invitrogen #R37117), Goat anti-Chicken Alexa 488 (ThermoFisher #A11039). For
545 co-localization analysis, only fibers for which > 50% of the length of the visible fiber contained co-localized
546 (white) pixels were counted. Image analysis was performed using FIJI.
547
548 *Whole mount skin IHC*
549 Staining was performed according to Marshall and Clary *et al*[71]. Briefly, 8-week-old mice were euthanized
550 and the back skin was shaved, depilated, and tape-stripped. The removed skin was fixed overnight in 4%
551 PFA, then washed in PBS (3X for 10 minutes each). Dermal fat was scraped away with a scalpel and skin
552 was washed in PBST (0.3% Triton X-100; 3X for two hours each) then incubated in 1:500 primary antibody

553 (Rabbit anti DsRed: Clontech #632496; Chicken anti-Nefh: Abcam #4680) in blocking buffer (PBST with
554 5% goat serum and 20% DMSO) for 5.5 days at 4°C. Skin was washed as before and incubated in 1:500
555 secondary antibody (Goat anti-Rabbit Alexa 594; Invitrogen #R37117; Goat anti-Chicken Alexa 488;
556 ThermoFisher #A11039) in blocking buffer for 3 days at 4°C. Skin was washed in PBST, serially dried in
557 methanol: PBS solutions, incubated overnight in 100% methanol, and finally cleared with a 1:2 solution of
558 benzyl alcohol: benzyl benzoate (BABB; Sigma) before mounting between No. 1.5 coverglass. Sectioned
559 and whole mount skin samples were imaged on a Zeiss LSM 880 confocal microscope with OPO using a
560 20x water objective. Image analysis was performed using FIJI.
561
562 *Cell culture*
563 Cell culture was carried out as previously described[72]. Briefly, neurons from dorsal root ganglia (2-8 week
564 old adults) or trigeminal ganglia (P0) were dissected and incubated for 10 min in 1.4 mg ml−1 Collagenase
565 P (Roche) in Hanks calcium-free balanced salt solution, followed by incubation in 0.25% standard trypsin
566 (vol/vol) STV versene-EDTA solution for 2 min with gentle agitation. Cells were then triturated, plated onto
567 Poly D-Lysine coated glass coverslips and used within 20 h. Media: MEM Eagle's with Earle's BSS
568 medium, supplemented with 10% horse serum (vol/vol), MEM vitamins, penicillin/streptomycin and L-
569 glutamine.
570
571 *Calcium imaging*
572 Ca^{2+} imaging experiments were carried out as previously described[72]. Cells were loaded for 60 min at room
573 temperature with 10 μM Fura-2AM supplemented with 0.01% Pluronic F-127 (wt/vol, Life Technologies) in
574 a physiological Ringer's solution containing (in mM) 140 NaCl, 5 KCl, 10 HEPES, 2 CaCl2, 2 MgCl2 and 10
575 D-(+)-glucose, pH 7.4. All chemicals were purchased from Sigma. Acquired images were displayed as the
576 ratio of 340 nm/ 380 nm. Cells were identified as neurons by eliciting depolarization with high potassium
577 Ringer's solution (75 mM) at the end of each experiment. Responding neurons were defined as those
578 having a > 15% increase from baseline ratio. Image analysis and statistics were performed using
579 automated routines in Igor Pro (WaveMetrics). Fura-2 ratios were normalized to the baseline ratio
580 F340/F380 = (Ratio)/(Ratio t = 0).

581

582 *In vitro electrophysiology*

583 Electrophysiological experiments were carried out as previously described[72]. Briefly, recordings were
584 collected at 5 kHz and filtered at 2 kHz (Axopatch 200B, pClamp software). Electrode resistance ranged
585 between 1.5–5 MΩ. Internal solution contained 140 mM KCl, 2 mM MgCl2, 1 mM EGTA, 5 mM HEPES, 1
586 mM Na2ATP, 100 μM GTP, and 100 μM cAMP (pH 7.4). Bath solution was physiological Ringer's solution.
587 The pipette potential was canceled before seal formation. Cell capacitance was canceled before whole cell
588 voltage-clamp recordings. For mechanonociceptors experiments, only cells which were visually identified
589 as mCherry expressing and which had a capacitance between 40-80 pF were used. Rheobase was
590 calculated as the smallest current step required to elicit an action potential using current steps of 50 pA. M
591 currents were measured and analyzed using standard protocols for DRG neurons reported in the
592 literature[30,32,73]. Experiments were carried out only on cells with a series resistance of less than 30
593 MΩ. Analysis of electrophysiology data was performed in pClamp and IgorPro.

594

595 *Ex vivo skin-nerve electrophysiology*

596 Touch-evoked responses in the skin were recorded after dissecting the hind limb skin and saphenous
597 nerve from 7-10 week old mice, according to published methods[74,75]. The skin was placed epidermis-side-
598 up in a custom chamber and perfused with carbogen-buffered synthetic interstitial fluid (SIF) kept at 32 °C
599 with a temperature controller (model TC-344B, Warner Instruments). The nerve was kept in mineral oil in a
600 recording chamber, teased apart, and placed onto a gold recording electrode connected with a reference
601 electrode to a differential amplifier (model 1800, A-M Systems). The extracellular signal was digitized using
602 a PowerLab 8/35 board (AD Instruments) and recorded using LabChart software (AD Instruments).

603

604 For these studies, we focused on A-mechanonociceptors (AMs). To identify responses from these afferents
605 in mutant and control genotypes, we used a mechanical search paradigm with a fine glass probe. Afferents
606 were classified as AMs according to the following criteria: (1) conduction velocity (approximately, 1 to (≤ 12
607 m/s^{-1}), (2) medium-sized receptive fields, (3) sustained response to mechanical indentation[74,76,77].

608

609 Touch-sensitive afferents that did not meet these criteria were not analyzed further. Responses were
610 classified as Adapting AMs if the ratio of mean firing rate in the dynamic phase of stimulation (first 0.2 s) to
611 the static phase of stimulation (last 4.8 s) was greater than 2, and Non-Adapting AMs if the ratio was less
612 than or equal to 2. Non-responders (**Figure 6F**) responded to suprathreshold mechanical stimulation with
613 von Frey monofilaments (tip diameter <0.5 mm), but not to maximal controlled mechanical stimulation (256
614 mN, tip diameter 2 mm). All recordings and analyses were performed blind to genotype.
615
616 Mechanical responses were elicited with von Frey monofilaments and a force controlled custom-built
617 mechanical stimulator. Mechanical thresholds were defined as the lowest von Frey monofilament to reliable
618 elicit at least on action potential. Force controlled mechanical stimuli were delivered using a computer
619 controlled, closed-loop, mechanical stimulator (Model 300C-I, Aurora Scientific, 2 mm tip diameter). Low-
620 pass filtered, 5-second long, length control steps (square wave) simultaneously delivered with permissive
621 force control steps (square wave) were generated using LabChart software (AD Instruments). An arbitrarily
622 selected force step-and-hold protocol (8, 32, 4, 64, 128, 16, 256 mN) was delivered to all fibers. The period
623 between successive displacements was 60 seconds.
624
625 Conduction velocity was measured by electrically stimulating identified receptive fields. Spike sorting by
626 principal component analysis (PCA) and density based clustering, and data analysis was performed off-line
627 with custom-made software in MATLAB. Statistics were performed in Prism.
628
629 *Flow cytometry of CFA-treated hind paws*
630 CFA injections were performed as described above. Briefly, hindpaw skin and underlying fascia of treated
631 and PBS-injected paws were removed from freshly euthanized mice. Skin was placed in RPMI media
632 (Gibco) on ice before mincing with dissection scissors. Digestions were performed for 90 minutes at 37°C
633 on a rotating platform in 1 mL RPMI supplemented with 1:1000 DNaseI enzyme (Roche) and 1 unit
634 LiberaseTM (Roche). Skin was then filtered through 70 µm nylon mesh (Falcon), washed in RPMI, and
635 resuspended in PBS for Aqua Live-Dead staining. Samples were then transferred to FACS buffer (PBS
636 with 0.5% FBS and 2 mM EDTA), blocked, then surface stained with the following antibodies: cKit-Biotin,

637 FceRI-PE, CD49b-PECy7, SiglecF-APC, SA-FITC, Ly6C-PerCP, CD11b-PB, Ly6G-BV785, CD45.2-
638 AF700. Compensation tubes (single-stain) were prepared for each fluorophore using positive and negative
639 control beads. A spleen from a wild-type animal was also prepared by crushing between frosted glass
640 slides, straining through 70 μm nylon mesh, and lysing of erythrocytes in ACK (Gibco). A portion of spleen
641 sample was heat-killed for 10 minutes at 65°C and stained with Aqua viability stain and set aside. The rest
642 of the spleen was stained normally with the other skin samples. Samples were then run through a flow
643 cytometer (BD Fortessa). Data were analyzed using FlowJo (Prism) and Microsoft Excel. Neutrophils were
644 defined as live single cells with the following staining profile: $CD45.2^{+}/CD11b^{+}/Ly6G^{+}/Ly6C^{+}$. Inflammatory
645 monocytes were defined as the following: $CD45.2^{+}/CD11b^{+}/Ly6G^{-}/Ly6C^{high}$. Total number of immune cells
646 was reported, rather than percentage of total, since neither genotype differed significantly in total number of
647 live cells or total number of $CD45.2^{+}$ immune cells.
648
649 *Statistical analyses*
650 All statistical analyses, except for skin nerve data (see above), were performed using IgorPro software or
651 Microsoft Excel. Values are reported as the mean ± SEM where multiple independent experiments are
652 pooled and reported (for whole cell electrophysiology), and mean ± SD where one experiment was
653 performed with multiple wells (for calcium imaging) or mice (for behavior). For comparison between two
654 groups, Student's unpaired 2-tailed t-test was used. A paired t-test was employed only for measurements
655 within the same biological replicate and after a given treatment. For single-point comparison between >2
656 groups, a one-way ANOVA followed by appropriate post hoc test was used, depending on comparison. For
657 the time course comparison between 2 groups, 2-way ANOVA was used and single comparison p-values
658 were derived using Tukey's HSD or appropriate statistical test, depending on comparison. Number of mice
659 or samples required to attain significance was not calculated beforehand, and where multiple statistical
660 tests were performed, a Bonferroni correction was applied. In figure legends, significance was labeled as:
661 n.s., not significant, $p \geq 0.05$; *$p < 0.05$; **$p < 0.01$; ***$p < 0.001$.
662
663
664

Acknowledgements

We thank Z. Rifi (UC Berkeley) for assistance with scoring itch behavior, R. P. Dalton (UC Berkeley) for assistance with confocal microscopy, and P. Lishko and M. Miller (UC Berkeley) for advice on lipid stability and usage. We would also like to thank R. Clary (Columbia) for whole mount skin staining protocols, B. Jenkins (Columbia) for advice on the immunohistochemistry experiments, and D. Julius (UC San Francisco) for the gift of Hm1a spider toxin. Confocal imaging experiments were conducted at the CRL Molecular Imaging Center, supported by the Helen Wills Neuroscience Institute (UC Berkeley). We would like to thank H. Aaron and J. Lee for their microscopy training and assistance. We are grateful to all members of the D.M.B Laboratory (UC Berkeley) for constructive feedback and criticism. The National Institutes of Health grants NS077224 (to D.M.B and R.B.), AR059385 (to D.M.B.), AR051219 (to E.A.L), NS105449 and GM007367 (to B.U.H), and NS063307 (to the Neurobiology Course at the Marine Biological Laboratory); and a Howard Hughes Medical Institute Faculty Scholars grant (to D.M.B) supported this work.

Competing interests

The authors declare no competing interests at this time.

References

1. Caterina, M. J. *et al.* Impaired Nociception and Pain Sensation in Mice Lacking the Capsaicin Receptor. *Science.* **288,** 306–313 (2000).
2. Vriens, J. *et al.* TRPM3 Is a Nociceptor Channel Involved in the Detection of Noxious Heat. *Neuron* **70,** 482–494 (2011).
3. Ranade, S. S. *et al.* Piezo2 is the major transducer of mechanical forces for touch sensation in mice. *Nature* **516,** 121–125 (2014).
4. Woo, S.H. *et al.* Piezo2 is required for Merkel-cell mechanotransduction. *Nature* **509,** 622–626 (2014).
5. Arcourt, A. *et al.* Touch Receptor-Derived Sensory Information Alleviates Acute Pain Signaling and Fine-Tunes Nociceptive Reflex Coordination. *Neuron* **93,** 179–193 (2017).
6. Ghitani, N. *et al.* Specialized Mechanosensory Nociceptors Mediating Rapid Responses to Hair Pull.

693 *Neuron* **95,** 944–954.e4 (2017).

694 7. Duan, B. *et al.* Identification of Spinal Circuits Transmitting and Gating Mechanical Pain. *Cell* **159,**
695 1417–1432 (2014).

696 8. Spiegel, S. & Milstien, S. Sphingosine-1-phosphate: an enigmatic signalling lipid. *Nat Rev Mol Cell*
697 *Biol* **4,** 397–407 (2003).

698 9. Matloubian, M. *et al.* Lymphocyte egress from thymus and peripheral lymphoid organs is dependent
699 on S1P receptor 1. *Nature* **427,** 355–360 (2004).

700 10. Schwab, S. R. *et al.* Lymphocyte sequestration through S1P lyase inhibition and disruption of S1P
701 gradients. *Science* **309,** 1735–1739 (2005).

702 11. Janes, K. *et al.* The development and maintenance of paclitaxel-induced neuropathic pain require
703 activation of the sphingosine 1-phosphate receptor subtype 1. *J. Biol. Chem.* **289,** 21082–21097
704 (2014).

705 12. Mair, N. *et al.* Genetic evidence for involvement of neuronally expressed S1P1 receptor in nociceptor
706 sensitization and inflammatory pain. *PLoS One* **6,** (2011).

707 13. Camprubi-Robles, M. *et al.* Sphingosine-1-phosphate-induced nociceptor excitation and ongoing
708 pain behavior in mice and humans is largely mediated by S1P3 receptor. *J Neurosci* **33,** 2582–2592
709 (2013).

710 14. Brinkmann, V. *et al.* Fingolimod (FTY720): discovery and development of an oral drug to treat
711 multiple sclerosis. *Nat Rev Drug Discov* **9,** 883–897 (2010).

712 15. Couttas, T. a *et al.* Loss of the neuroprotective factor Sphingosine 1-phosphate early in Alzheimer's
713 disease pathogenesis. *Acta Neuropathol. Commun.* **2,** 9 (2014).

714 16. Finley, A. *et al.* Sphingosine 1-phosphate mediates hyperalgesia via a neutrophil-dependent
715 mechanism. *PLoS One* **8,** e55255 (2013).

716 17. Weth, D. *et al.* Activated platelets release sphingosine 1-phosphate and induce hypersensitivity to
717 noxious heat stimuli in vivo. *Front. Neurosci.* **9,** 1–8 (2015).

718 18. Weth-Malsch, D. *et al.* Ablation of Sphingosine 1-Phosphate Receptor Subtype 3 Impairs
719 Hippocampal Neuron Excitability In vitro and Spatial Working Memory In vivo. *Front. Cell. Neurosci.*
720 **10,** 1–12 (2016).

721 19. Usoskin, D. *et al.* Unbiased classification of sensory neuron types by large-scale single-cell RNA
722 sequencing. *Nat. Neurosci.* **18,** 145–153 (2015).
723 20. Zhang, Y. H., Fehrenbacher, J. C., Vasko, M. R. & Nicol, G. D. Sphingosine-1-phosphate via
724 activation of a G-protein-coupled receptor(s) enhances the excitability of rat sensory neurons. *J.*
725 *Neurophysiol.* **96,** 1042–1052 (2006).
726 21. Li, C., Li, J., Kays, J., Guerrero, M. & Nicol, G. D. Sphingosine 1-phosphate enhances the excitability
727 of rat sensory neurons through activation of sphingosine 1-phosphate receptors 1 and/or 3. *J.*
728 *Neuroinflammation* **12,** 1–20 (2015).
729 22. Gerhold, K. *et al.* The Star-Nosed Mole Reveals Clues to the Molecular Basis of Mammalian Touch.
730 *PLoS One* **8,** (2013).
731 23. Kono, M. *et al.* The sphingosine-1-phosphate receptors S1P1, S1P2, and S1P3 function coordinately
732 during embryonic angiogenesis. *J. Biol. Chem.* **279,** 29367–29373 (2004).
733 24. Nussbaum, C. *et al.* Sphingosine-1-phosphate receptor 3 promotes leukocyte rolling by mobilizing
734 endothelial P-selectin. *Nat. Commun.* **6,** 6416 (2015).
735 25. Chiba, Y., Takeuchi, H., Sakai, H. & Misawa, M. SKI-II, an inhibitor of sphingosine kinase,
736 ameliorates antigen-induced bronchial smooth muscle hyperresponsiveness, but not airway
737 inflammation, in mice. *J. Pharmacol. Sci.* **114,** 304–310 (2010).
738 26. Shaner, R. L. *et al.* Quantitative analysis of sphingolipids for lipidomics using triple quadrupole and
739 quadrupole linear ion trap mass spectrometers. *J. Lipid Res.* **50,** 1692–1707 (2009).
740 27. Sanna, M. *et al.* Bitopic S1P3 Antagonist Rescue from Complete Heart Block: Pharmacological and
741 Genetic Evidence for Direct S1P3 Regulation of Mouse Cardiac Conduction. *Mol. Pharmacol.* **89,**
742 176–186 (2015).
743 28. Osteen, J. D. *et al.* Selective spider toxins reveal a role for the Nav1.1 channel in mechanical pain.
744 *Nature* **534,** 494–9 (2016).
745 29. Joost, S. *et al.* Single-Cell Transcriptomics Reveals that Differentiation and Spatial Signatures
746 Shape Epidermal and Hair Follicle Heterogeneity. *Cell Syst.* **3,** 221–237.e9 (2016).
747 30. Schutze, S., Orozco, I. J. & Jentsch, T. J. KCNQ Potassium Channels Modulate Sensitivity of Skin
748 Down hair (D-hair) Mechanoreceptors. *J. Biol. Chem.* **291,** 5566–5575 (2016).

749 31. Passmore, G. M. *et al.* Functional significance of M-type potassium channels in nociceptive
750 cutaneous sensory endings. *Front. Mol. Neurosci.* **5,** 1–12 (2012).
751 32. Crozier, R. A., Ajit, S. K., Kaftan, E. J. & Pausch, M. H. MrgD Activation Inhibits KCNQ / M-Currents
752 and Contributes to Enhanced Neuronal Excitability. *J Neurosci* **27,** 4492–4496 (2007).
753 33. Xu, W. *et al.* Activation of Voltage-Gated KCNQ/Kv7 Channels by Anticonvulsant Retigabine
754 Attenuates Mechanical Allodynia of Inflammatory Temporomandibular Joint in Rats. *Mol. Pain* **6,**
755 1744-8069-6–49 (2010).
756 34. Ramos-Perez, W. D., Fang, V., Escalante-Alcalde, D., Cammer, M. & Schwab, S. R. A map of the
757 distribution of sphingosine 1-phosphate in the spleen. *Nat. Immunol.* **16,** 1245–52 (2015).
758 35. McIlwrath, S. L., Lawson, J. J., Anderson, C. E., Albers, K. M. & Koerber, H. R. Overexpression of
759 neurotrophin-3 enhances the mechanical response properties of slowly adapting type 1 afferents
760 and myelinated nociceptors. *Eur. J. Neurosci.* **26,** 1801–1812 (2007).
761 36. Kwan, K. Y., Glazer, J. M., Corey, D. P., Rice, F. L. & Stucky, C. L. TRPA1 Modulates
762 Mechanotransduction in Cutaneous Sensory Neurons. *J. Neurosci.* **29,** 4808–4819 (2009).
763 37. Smith, A. K., O'Hara, C. L. & Stucky, C. L. Mechanical sensitization of cutaneous sensory fibers in
764 the spared nerve injury mouse model. *Mol. Pain* **9,** 1–6 (2013).
765 38. Garrison, S. R., Dietrich, A. & Stucky, C. L. TRPC1 contributes to light-touch sensation and
766 mechanical responses in low-threshold cutaneous sensory neurons. *J. Neurophysiol.* **107,** 913–922
767 (2012).
768 39. Ghasemlou, N., Chiu, I. M., Julien, J.-P. & Woolf, C. J. CD11b $^{+}$ Ly6G $^{-}$ myeloid cells mediate
769 mechanical inflammatory pain hypersensitivity. *Proc. Natl. Acad. Sci.* 201501372 (2015).
770 doi:10.1073/pnas.1501372112
771 40. Abrahamsen, B. *et al.* The Cell and Molecular Basis of Mechanical, Cold, and Inflamatory Pain.
772 *Science.* **321,** 702 (2008).
773 41. Lennertz, R. C., Kossyreva, E. A., Smith, A. K. & Stucky, C. L. TRPA1 mediates mechanical
774 sensitization in nociceptors during inflammation. *PLoS One* **7,** 1–11 (2012).
775 42. Chalfant, C. E. & Spiegel, S. Sphingosine 1-phosphate and ceramide 1-phosphate: expanding roles
776 in cell signaling. *J. Cell Sci.* **118,** 4605–4612 (2005).

777 43. Pappu, R. *et al.* Promotion of lymphocyte egress into blood and lymph by distinct sources of
778 sphingosine-1-phosphate. *Science* **316,** 295–298 (2007).
779 44. Morita, T. *et al.* HTR7 Mediates Serotonergic Acute and Chronic Itch. *Neuron* **87,** 124–138 (2015).
780 45. Szczot, M. *et al.* Cell-Type-Specific Splicing of Piezo2 Regulates Mechanotransduction. *Cell Rep.*
781 **21,** 2760–2771 (2017).
782 46. Passmore, G. M. *et al.* KCNQ/M currents in sensory neurons: significance for pain therapy. *J.*
783 *Neurosci.* **23,** 7227–7236 (2003).
784 47. Hayashi, H., Iwata, M., Tsuchimori, N. & Matsumoto, T. Activation of peripheral KCNQ channels
785 attenuates inflammatory pain. *Mol. Pain* **10,** 15 (2014).
786 48. Blackburn-Munro, G. & Jensen, B. S. The anticonvulsant retigabine attenuates nociceptive
787 behaviours in rat models of persistent and neuropathic pain. *Eur. J. Pharmacol.* **460,** 109–116
788 (2003).
789 49. Ray, P. *et al.* Comparative transcriptome profiling of the human and mouse dorsal root ganglia: An
790 RNA-seq-based resource for pain and sensory neuroscience research. *bioRxiv* 165431 (2017).
791 doi:10.1101/165431
792 50. Flegel, C. *et al.* RNA-Seq analysis of human trigeminal and dorsal root ganglia with a focus on
793 chemoreceptors. *PLoS One* **10,** 1–30 (2015).
794 51. Young, G. T. *et al.* Characterizing human stem cell-derived sensory neurons at the single-cell level
795 reveals their ion channel expression and utility in pain research. *Mol. Ther.* **22,** 1530–1543 (2014).
796 52. Oetjen, L. K. *et al.* Sensory Neurons Co-opt Classical Immune Signaling Pathways to Mediate
797 Chronic Itch. *Cell* **129,** 742–751 (2017).
798 53. Pinho-Ribeiro, F. A., Verri, W. A. & Chiu, I. M. Nociceptor Sensory Neuron–Immune Interactions in
799 Pain and Inflammation. *Trends Immunol.* **38,** 5–19 (2017).
800 54. Donoviel, M. S. *et al.* Spinster 2, a sphingosine 1-phosphate transporter, plays a Critical Role in
801 inflammatory and Autoimmune Diseases. *FASEB J.* **29,** 5018–5028 (2015).
802 55. Gräler, M. H. & Goetzl, E. J. The immunosuppressant FTY720 down-regulates sphingosine 1-
803 phosphate G-protein-coupled receptors. *FASEB J.* **18,** 551–553 (2004).
804 56. Olivera, A., Allende, M. L. & Proia, R. L. Shaping the landscape: Metabolic regulation of S1P

805 gradients. *Biochim. Biophys. Acta - Mol. Cell Biol. Lipids* **1831,** 193–202 (2013).

806 57. Allende, M. L. *et al.* Sphingosine-1-phosphate lyase deficiency produces a pro-inflammatory
807 response while impairing neutrophil trafficking. *J. Biol. Chem.* **286,** 7348–7358 (2011).

808 58. Kunkel, G. T., Maceyka, M., Milstien, S. & Spiegel, S. Targeting the sphingosine-1-phosphate axis in
809 cancer, inflammation and beyond. *Nat. Rev. Drug Discov.* **12,** 688–702 (2013).

810 59. Roviezzo, F. *et al.* S1P-induced airway smooth muscle hyperresponsiveness and lung inflammation
811 in vivo: Molecular and cellular mechanisms. *Br. J. Pharmacol.* **172,** 1882–1893 (2015).

812 60. Liang, J. *et al.* Sphingosine-1-Phosphate Links Persistent STAT3 Activation, Chronic Intestinal
813 Inflammation, and Development of Colitis-Associated Cancer. *Cancer Cell* **23,** 107–120 (2013).

814 61. Rivera, J., Proia, R. L. & Olivera, A. The alliance of sphingosine-1-phosphate and its receptors in
815 immunity. *Nat. Rev. Immunol.* **8,** 753–763 (2008).

816 62. Myśliwiec, H. *et al.* Increase in circulating sphingosine-1-phosphate and decrease in ceramide levels
817 in psoriatic patients. *Arch. Dermatol. Res.* (2016). doi:10.1007/s00403-016-1709-9

818 63. Checa, A. *et al.* Circulating levels of sphingosine-1-phosphate are elevated in severe, but not mild
819 psoriasis and are unresponsive to anti-TNF-α treatment. *Sci. Rep.* **5,** 12017 (2015).

820 64. Grenald, S. A. *et al.* Targeting the S1P/S1PR1 axis mitigates cancer-induced bone pain and
821 neuroinflammation. *Pain* **158,** 1 (2017).

822 65. Trankner, D., Hahne, N., Sugino, K., Hoon, M. A. & Zuker, C. Population of sensory neurons
823 essential for asthmatic hyperreactivity of inflamed airways. *Proc. Natl. Acad. Sci.* **111,** 11515–11520
824 (2014).

825 66. Wilson, S. R. *et al.* The Ion Channel TRPA1 Is Required for Chronic Itch. *J. Neurosci.* **33,** 9283–
826 9294 (2013).

827 67. Tsunozaki, M. *et al.* A 'toothache tree' alkylamide inhibits Aδ mechanonociceptors to alleviate
828 mechanical pain. *J. Physiol.* **591,** 3325–40 (2013).

829 68. Shimada, S. G. & LaMotte, R. H. Behavioral differentiation between itch and pain in mouse. *Pain*
830 **139,** 681–687 (2008).

831 69. Chaplan, S.R., Bach, F.W., Pogrel, J.W., Chung, J.M., Yaksh, T. Quantitative assessment of tactile
832 allodynia evoked by unilateral ligation of the fifth and sixth lumbar nerves in the rat. *J. Neurosci.* **53,**

833 55–63 (1994).

834 70. Dixon, W. J. The Up-and-Down Method for Small Samples. *J. Am. Stat. Assoc.* **60,** 967–978 (1980).

835 71. Marshall, K. L. *et al.* Touch Receptors Undergo Rapid Remodeling in Healthy Skin. *Cell Rep.* **17,**
836 1719–1727 (2016).

837 72. Wilson, S. R. *et al.* TRPA1 is required for histamine-independent, Mas-related G protein-coupled
838 receptor-mediated itch. *Nat. Neurosci.* **14,** 595–602 (2011).

839 73. Zheng, Q. *et al.* Suppression of KCNQ/M (Kv7) potassium channels in dorsal root ganglion neurons
840 contributes to the development of bone cancer pain in a rat model. *Pain* **154,** 434–448 (2013).

841 74. Wellnitz, S. A., Lesniak, D. R., Gerling, G. J. & Lumpkin, E. A. The Regularity of Sustained Firing
842 Reveals Two Populations of Slowly Adapting Touch Receptors in Mouse Hairy Skin. *J.*
843 *Neurophysiol.* **103,** 3378–3388 (2010).

844 75. Maksimovic, S. *et al.* Epidermal Merkel cells are mechanosensory cells that tune mammalian touch
845 receptors. *Nature* **509,** 617–621 (2014).

846 76. Koltzenburg, M. *et al.* Receptive Properties of Mouse Sensory Neurons Innervating Hairy Skin
847 Receptive Properties of Mouse Sensory Neurons Innervating Hairy Skin. *J. Neurophysiol.* **78,** 1841–
848 1850 (1997).

849 77. Zimmermann, K. *et al.* Phenotyping sensory nerve endings in vitro in the mouse. *Nat. Protoc.* **4,**
850 174–196 (2009).

851

852 ## Figure captions

853 **Figure 1. S1PR3 mediates acute mechanical pain. A.** von Frey 50% withdrawal threshold
854 measurements for *S1pr3*$^{+/+}$ (WT, N = 8), $^{+/-}$ (HET, N = 7) and $^{-/-}$ (KO, N = 12) mice. $p < 0.0001$ (one-way
855 ANOVA). Tukey-Kramer post hoc comparisons for KO and HET to WT indicated on graph. **B.** von Frey
856 force-response graph for WT (N = 8) versus KO (N = 12) animals; $p_{genotype} < 0.0001$ (two-way ANOVA).
857 Tukey HSD comparisons between genotypes are indicated for given forces. **C.** % withdrawal to pinprick
858 stimulation of hindpaw for HET versus KO animals; $p < 0.0001$ (unpaired t-test; N = 5-7 mice per group). **D.**
859 Number of attempted removal bouts in tape assay for WT (N =2), HET (N = 2), and KO (N = 5) mice; $p =$
860 0.172 (one-way ANOVA). **E.** Baseline radiant heat measurements for WT, HET, and KO mice. N = 8 WT, 3

861 HET, and 5 KO mice. p = 0.444 (one-way ANOVA). **F.** von Frey 50% withdrawal threshold measurements
862 for mice pre- and post-injection of 500 μM TY 52156 (N = 10), 10 μM W146 (N = 6), or 1% DMSO-PBS
863 vehicle (N = 17); p = 0.016, 0.650 (two-tailed paired t-test comparing vehicle- vs. drug-injected paw). **G.**
864 von Frey force-response graph for mice injected with either 1% DMSO-PBS or 500 μM TY 52156; $p_{treatment}$ <
865 1e-05 (two-way ANOVA; N = 4 mice per group). Tukey HSD comparisons were made between treatment
866 groups and significant differences at a given force are indicated on graph. Error bars represent mean ± SD.
867
868 **Figure 1-source data 1. S1PR3 mediates acute mechanical pain.** *Related to Figure 1.*
869
870 **Figure 1-figure supplement 1. Loss of S1PR3 selectively impairs mechanonociception.** *Related to*
871 *Figure 1.* **A.** Time to righting in seconds for N = 6 P7 pups per genotype for WT and KO mice; p = 0.575
872 (two-tailed unpaired t-test). **B.** (Left) Time spent scratching in response to injection of 50 mM chloroquine or
873 PBS vehicle (VEH) in WT and KO mice; p = 0.36, 0.98, (unpaired t-tests; N = 3-4 mice per group). (Right)
874 Time spent scratching in response to injection of 27 mM Histamine or 0.1% DMSO-PBS in WT and KO
875 mice; p = 0.51, 0.06 (unpaired t-tests; N = 3-4 mice per group). **C.** Normalized paw withdrawal latencies
876 post-injection of SKI II, TY 52156, or 0.1% DMSO-PBS vehicle into the hind paw of wild-type animals; p =
877 0.65 (one-way ANOVA); N = 5 mice per group. Unless otherwise indicated, error bars represent mean ±
878 SD.
879
880 **Figure 2. Endogenous S1P mediates acute mechanical pain. A.** von Frey 50% withdrawal
881 measurements for mice pre- and post-injection of 50 μM SKI II (N = 8) or 10 μM S1P (N = 7); p = 0.003,
882 0.604 (two-tailed paired t-tests). **B.** von Frey force-response graph for animals injected with 10 μM S1P or
883 0.1% MeOH-PBS; $p_{genotype}$ > 0.05 (two-way ANOVA; N = 8 mice per group). No Tukey HSD comparisons
884 at any force between genotypes were significant. **C.** Intradermal cheek injection of 10 μM S1P, 2 μM, 0.2
885 μM, and 20 μL 0.3% methanol PBS (vehicle), with quantification of number of forepaw wipes over the 5
886 minute post-injection interval; p < 0.0001 (one-way ANOVA; N = 3 mice per condition). Dunnett's multiple
887 comparisons p-values are represented on graph for comparisons made between treated and vehicle
888 groups. **D.** Radiant heat normalized paw withdrawal latencies 20-30 minutes post injection of 15 μL 10 μM

889 S1P, 0.2 μM S1P. or 0.3% methanol-PBS vehicle (i.d.) into the hind paw of S1PR3 WT or KO mice; *p* =
890 0.0129 (one-way ANOVA; N = 3-10 mice per condition). Dunnett's multiple comparisons *p*-values are
891 represented on graph for comparisons made between treated and vehicle groups. **E.** von Frey 50%
892 withdrawal measurements for mice pre- (baseline) and post-injection of 50 μM SKI II (N = 14) and 0, 10,
893 75, or 200 nM S1P (one-way ANOVA, p = 0.0001; N = 4, 3, 4, 3 animals). Tukey Kramer comparisons are
894 indicated on graph. Error bars represent mean ± SD.
895
896 **Figure 2-source data 1. Endogenous S1P mediates acute mechanical pain.** *Related to Figure 2.*
897
898 **Figure 3. *S1pr3* is expressed in A mechanonociceptors and C thermal nociceptors. A.** (Top)
899 Representative co-ISH of *S1pr3* (green; left) with *Scn1a*, *Npy2r*, *Piezo2*, and *Trpv1* (magenta; center) in
900 sectioned DRG. Right column: overlay with co-localized regions colored white (10x air objective; scale =
901 100 μm). **B.** Bar chart showing the % of total cells expressing the indicated marker (grey) and the % of total
902 cells co-expressing both marker and *S1pr3* (green). See Table S1 for quantification. **C.** Representative IHC
903 images of sectioned DRG from *S1pr3*$^{mCherry/+}$ animals stained with anti-DsRed (green, S1PR3) and anti-
904 Peripherin (left, magenta) or anti-NF200 (right, magenta). Arrows indicate co-stained cells. Images were
905 acquired using a 10x air objective (scale = 100 μm). **D.** Whole-mount skin IHC confocal images with anti-
906 DsRed antibody (S1PR3, green) and anti-NefH antibody (NF200, magenta) in an *S1pr3*$^{mCherry/+}$ animal (20x
907 water objective; scale = 50 μm). Arrows indicate co-positive free nerves (left image). Arrowheads indicate
908 NF200- free nerves (left) or S1PR3- circumferential fibers (right image). **E.** Sectioned skin IHC with anti-
909 DsRed (S1PR3) and anti-NefH (NF200, left, top right) or anti-DsRed (S1PR3) and anti-beta-tubulin III
910 (BTIII, bottom right) antibody (magenta) in *S1pr3*$^{mCherry/+}$ skin (20x air objective; scale = 50 μm). Arrows
911 indicate co-positive free nerve endings (left), S1PR3-negative lanceolate/circumferential hair follicle
912 endings (top right, arrow = circumferential, arrowhead = lanceolate), or S1PR3-negative putative Merkel
913 afferent (bottom right). **F.** (Left) Quantification of sectioned DRG IHC experiments showing % of S1PR3+
914 cells that co-stained with indicated markers (n > 250 cells per marker). (Right) Quantification of sectioned
915 skin IHC experiments showing % of fibers positive for indicated marker that co-stained with S1PR3 (anti-
916 DsRed; n = 10 images per marker from 2 animals).

917

918 **Figure 3-figure supplement 1. S1PR3 KO animals display normal representation of somatosensory**
919 **neuronal subtypes.** *Related to Figure 3.* **A.** ISH of sectioned adult DRG from WT and S1PR3 KO animals
920 showing specificity of *S1pr3* probes (20x air objective, scale = 50 μm). **B.** (Image) Representative ISH
921 *Trpv1* (top) and *Trpa1* (bottom) from sectioned DRG of wild-type (left) and S1PR3 KO animals (right; 20x
922 air objective; scale = 50 μm). **C.** % of total cells expressing *Trpv1* and *Trpa1* in sectioned DRG of wild-type
923 and S1PR3 KO animals. **D.** (Left) Average diameter ± SEM of all cells in sectioned DRG from WT and
924 S1PR3 KO animals (p = 0.36, t-test; n = 437 and 679 cells from two animals each, respectively). (Right)
925 Average diameter ± SD of *Trpv1+* cells in WT and S1PR3 KO DRG (p = 0.63, t-test; n = 127 and 85 cells
926 respectively). **E.** Representative staining with anti-S1PR3 antibody (1:2000) in sectioned adult DRG from
927 WT and S1PR3 KO animals (10x air objective, scale = 100 μm). **F.** Representative IHC images of
928 sectioned DRG from S1PR3 KO animals stained with anti-DsRed (green) and anti-Peripherin (left,
929 magenta) or anti-NF200 (right, magenta). Images were acquired using a 10x air objective (scale = 100 μm).
930 **G.** (Left) Quantification of total percentage of cells stained with indicated markers in sectioned DRG from
931 *S1pr3*$^{mCherry/+}$ and S1PR3 KO animals (n > 250 cells per condition). (Right) Average diameter of anti-
932 NF200+ cells in *S1pr3*$^{mCherry/+}$ and S1PR3 KO DRG (p = 0.15, t-test; n = 256 and 194 cells, respectively). **H.**
933 Percent responders to S1P and capsaicin in ratiometric calcium imaging of wild-type and *S1pr3* $^{-/-}$ cultured
934 DRG and TG neurons; $p < 0.0001$ (one-way ANOVA; N = 2 DRG and 2 TG preparations of 8 wells each).
935 Sidak's multiple comparisons p-values are represented on graph for comparisons made between
936 genotypes. Error bars represent mean ± SEM. **I.** (Left) No primary control showing robust staining of hair
937 follicles in whole mount skin in contrast to specific neuronal staining shown in **Figure 3D**. (Right) No
938 primary control showing staining around hair follicles and in epidermis in sectioned skin. Scale = 50 μm
939 (20x water objective).

940

941 **Supplementary file 1. Co-ISH quantification for sectioned DRG from adult wild-type mice.** *Related to*
942 *Figure 3.*

943

944 **Figure 4. S1P activates thermal nociceptors but not mechanonociceptors. A.** (Left) Representative

945 image of mCherry signal in live, cultured adult DRG neurons from one *S1pr3*$^{mCherry/+}$ animal. (Right)
946 Quantification of % of total cells expressing *S1pr3* from DRG ISH and mCherry from dissociated DRG
947 cultures (N = 2 animals each experiment). **B.** Representative traces depicting F340/F380 signal from
948 Fura2-AM calcium imaging showing two neurons, one which responded to 1 μM S1P, 1 μM Capsaicin, and
949 high K+ Ringer's (red) and one which only responded to high K+ (black). **C.** (Left) Fura-2 AM calcium
950 imaging before (left) and after (center) addition of 1 μM S1P in *S1pr3* $^{mCherry/+}$ cultured mouse DRG neurons.
951 Bar indicates fluorescence ratio. Right-hand image indicates mCherry fluorescence. (Right) % of mCherry
952 neurons that are responsive to 1 μM S1P in ratiometric calcium imaging (n > 1000 cells from 16 imaging
953 wells from three animals). **D.** Dose-response curve of mean neuronal calcium responders to varying
954 concentrations of S1P. Concentrations used: 1, 10, 50, 100, 200, 1000, and 10,000 nanomolar. Error bars
955 represent mean ± SD (N = 2 animals). Black dotted line indicates sigmoidal fit for all S1P responders from
956 which EC_{50} was derived. All S1P responders were also capsaicin-responsive. **E.** Current-clamp trace of a
957 single wild-type neuron firing action potentials in response to bath addition of 1 μM S1P and 1 μM
958 capsaicin, with Ringer's wash in-between. n = 4 of 10 neurons responded to S1P and N = 1 of 1 S1P-
959 responsive also responded to capsaicin. Bar = 2 seconds. **F.** (Left) Fura-2 AM calcium imaging after
960 addition of 500 nM Hm1a in *S1pr3*$^{mCherry/+}$ P0 TG neurons, which were instead of adult DRG neurons
961 because they respond to Hm1a without prior PGE_2 sensitization. Right-hand image indicates mCherry
962 fluorescence. (Right) % of Hm1a-responsive P0 TG neurons that are mCherry+ (N = 1 animal, 1230 total
963 neurons).
964

965 **Figure 5. S1PR3 modulates KCNQ2/3 channels to regulate AM excitability.** All experiments were
966 performed in *S1pr3*$^{mCherry/+}$ or $^{-/-}$ DRG neurons. **A.** (Left) Example traces of a single mCherry+ neuron in
967 whole cell current clamp before and after S1P application. (Right) % change in rheobase after S1P
968 application for *S1pr3*$^{mCherry/+}$ (left) and KO (right) neurons ($p_{WT,KO}$ = 0.012, 0.287; two-tailed paired t-tests; N
969 = 7, 12 cells). **B.** % Δ in input resistance after S1P or vehicle application (p = 0.017; two-tailed paired t-
970 test; N = 4 cells per group). **C.** The S1P-sensitive current is carried by potassium. The current-voltage
971 relationship was determined by subtraction of the post-S1P current from the pre-S1P current and reverses
972 at -60.125 mV; N = 6 cells. Data were fitted with a Boltzmann equation. Pre- and post-S1P currents were

973 measured at the indicated voltage (-100 mV to +80 mV, 20 mV increments) following a +100 mV step (100
974 ms). Current was quantified using the peak absolute value of the slowly-deactivating current 0-10 ms after
975 stepping to indicated voltage. Unless indicated otherwise, all error bars represent mean ± SEOM. **D.**
976 (Graphic, top) Averaged current traces of a single mCherry+ neuron in whole cell voltage clamp recording
977 comparing tail currents ($\Delta_{I\ tail}$) pre- and post-S1P using indicated voltage step protocol. (graphic, bottom)
978 Averaged current traces of a single mCherry+ neuron in whole cell voltage clamp recording with XE991
979 treatment. Holding phase (-40 mV, 150 ms) was truncated in traces. (Left graph) % Δ in outward tail current
980 (average +/- SD after indicated treatments (1 μM S1P, 3 μM XE 991, or both) for *S1pr3*$^{mCherry/+}$ medium-
981 diameter neurons; (p = 0.58; one-way ANOVA; n = 6, 8, 14 cells) using protocol depicted at right. (Right
982 graph) % Δ in inward tail current after indicated treatments (LINO = 100 μM linopirdine) for *S1pr3*$^{mCherry/+}$
983 medium-diameter neurons; (p = 0.47; two-tailed paired t-test; N = 12 cells).
984
985 **Figure 5-source data 1. S1PR3 modulates KCNQ2/3 channels to regulate AM excitability.** *Related to*
986 *Figure 5.*
987
988 **Figure 5-figure supplement 1. S1P selectively modulates potassium tail currents to increase DRG**
989 **neuron excitability.** *Related to Figure 5.* **A.** (Left) Example trace of a single mCherry+ neuron in S1P
990 before and after current injection. (Right) Resting membrane potential (RMP) in millivolts before and after
991 addition of S1P (p = 0.23; two-tailed paired t-test; n = 6 cells). **B.** Rheobase pre- and post-S1P application
992 in DRG neurons; p_{WT} = 0.011; p_{KO} = 0.28 (two-tailed paired t-test). Same data are represented in **Figure**
993 **5A**. **C.** Sodium I-V relationship for a representative *S1pr3*$^{mCherry/+}$ medium-diameter neuron pre- and 5
994 minutes post- 1 μM S1P using voltage step from -100 to +80 mV (150 ms steps, -80 mV holding). **D.**
995 Steady-state I-V relationship for same neuron. **E.** (Left) % Δ in peak sodium current (Na^+) after S1P or 1%
996 DMSO vehicle application for medium-diameter mCherry+ neurons; p = 0.39 (two-tailed paired t-test; n = 7
997 cells per group). (Right) % Δ in peak steady-state current (S.S. K^+) after S1P or 1% DMSO vehicle
998 application for medium-diameter mCherry+ neurons; p = 0.948 (two-tailed paired t-test; n = 7 cells per
999 group). **F.** % Δ in inward tail current ($\Delta_{I\ tail}$) after S1P or 1% DMSO vehicle application for *S1pr3*$^{mCherry/+}$ and
1000 KO medium-diameter neurons using a pre-pulse stimulation of +80 mV followed by a step to -80 mV, where

1001 ($\Delta_{I\ tail}$) was calculated by subtracting the steady-state current from the absolute peak of the slowly-
1002 deactivating current at -80 mV (p = 0.014; one-way ANOVA; N = 10, 13, 10 cells). Tukey Kramer post hoc
1003 p-values indicated on graph. **G.** Dose-response relationship between % Δ in tail current and S1P
1004 concentration for 1 nM, 50 nM, 100 nM, and 1 μM S1P (n = 7 cells). EC_{50} (48.8 nM), marked by thin dotted
1005 lines, was estimated from sigmoidal fit (thick dotted line).
1006
1007 **Figure 6. S1PR3 is required for nociceptive responses of high-threshold AM nociceptors.**
1008 **A.** (Left) Representative traces of AM fiber activity over time in *ex vivo* skin-saphenous nerve recording in
1009 response to stimulation (128 mN, top) from HET (middle) and KO (bottom) mice. (Right) Mean firing rate of
1010 AM fibers in response to force controlled stimulation (4, 8, 16, 32, 64, 128, 256 mN). **p=0.001,
1011 ***p=0.0002 (two-way ANOVA, Sidak's post-hoc); lines, linear regression (HET: slope=50 Hz/N, R^2=0.99;
1012 KO: slope=35 Hz/N, R^2=0.95). **B.** von Frey threshold of AM fibers in S1PR3 HET and KO specimens. ***p
1013 < 0.0001 (Mann-Whitney test); lines, median; boxes, 25-75 percentile; whiskers, min-max. **C.** Cumulative
1014 response plot of AM fibers to force controlled stimulation (solid lines); four-parameter logistic fit from which
1015 half-maximal force was estimated for each genotype (dotted lines). **D.** Conduction velocity (CV) of AM
1016 fibers in S1PR3 HET and KO mice. p = 0.65 (two-tailed t-test); n = 40, 36 fibers; errors, mean ± SEM. **E.**
1017 Representative traces and binned instantaneous firing frequencies (IFF; 200-ms bins) of Non-Adapting
1018 and Adapting AMs in response to force controlled stimulation (256 mN, top) for S1PR3 HET and KO mice;
1019 blue regions, dynamic phase of stimulation (200-ms). **F**. Proportion of fibers classified by pattern of
1020 mechanically evoked responses to 256-mN stimuli: Non-Responder (HET, 2/40 fibers; KO 5/36), Non-
1021 Adapting AM (HET, 18/40; KO, 29/36), Adapting AM (HET, 20/40; KO, 2/36). Non-Responders fired action
1022 potentials to large magnitude von Frey monofilaments (<0.5 mm tip diameter), but not controlled
1023 mechanical stimulation (256 mN, 2-mm tip diameter). ***p<0.00001 (Chi-square test).
1024
1025 **Figure 6-source data 1. S1PR3 is required for nociceptive responses of high-threshold AM**
1026 **nociceptors.** *Related to Figure 6.* Table provides properties of all S1PR3 HET and KO AM fibers that were
1027 recorded.
1028

1029 **Figure 6-figure supplement 1. S1PR3 HET AM nociceptors display normal nociceptive responses.**
1030 *Related to Figure 6*. **A.** Mean firing rate of AM fibers in response to force controlled stimulation (4, 8, 16,
1031 32, 64, 128, 256 mN) from **Figure 6A**, with additional data from one wild-type animal (n_{WT} = 4 fibers) (WT:
1032 slope, 57 Hz/N, R^2, 0.98; p = 0.90, two-way ANOVA comparing HET and WT). **B.** (Left) Conduction
1033 velocities from teased fibers from 6 S1PR3 KO animals (purple, Aβ, centroid=13.1 m/s; yellow, Aδ,
1034 centroid=5.7 m/s; orange, C, centroid=0.4 m/s; R^2 =0.69, N = 65 fibers). (Right) Conduction velocities from
1035 teased fibers from 1 S1PR3 HET and 6 C57BL/6 WT animals (purple, Aβ, centroid=14.5 m/s; yellow, Aδ,
1036 centroid=6.8 m/s; orange, C, centroid=0.3 m/s; R^2 =0.82, N = 76 fibers). Three-term Gaussian model. X-
1037 axis plotted on a log 1.2 scale. **C.** Mean firing rates during dynamic (ramp) and static (hold) stimulation for
1038 S1PR3 HET and S1PR3 KO recordings (left, Adapting AMs; right, Non-Adapting AMs; see **Figure 6E-F** for
1039 experimental details). No significant differences were found between genotypes (p = 0.227, 0.490 (two-way
1040 ANOVA); bars, means). As shown in **Figure 6F**, the proportion of Adapting AMs was significantly lower in
1041 S1PR3 KO recordings compared with littermate controls.
1042
1043 **Figure 7. S1PR3 is dispensable for development of chronic mechanical hypersensitivity. A.** Thermal
1044 latency before and after CFA treatment (indicated by dotted line); $p_{genotype}$ = 0.0053 (two-way ANOVA; N = 5
1045 mice per genotype). Sidak's multiple comparison between genotypes for specific time points indicated on
1046 graph. Error bars represent mean ± SD. **B.** (Left) Normalized 50% withdrawal threshold before and after
1047 CFA treatment (indicated by dotted line); p(genotype) < 0.001 (two-way ANOVA). (Right) 50% withdrawal
1048 thresholds for same experiment (p(genotype) = 0.1634; two-way ANOVA). **C.** (Left) Thermal latency
1049 assessed before ("Baseline") and 24 hours post CFA injection with either vehicle (CFA + VEH) or TY 52156
1050 (CFA + TY) acutely administered; p < 0.0001 (one-way ANOVA N = 5 mice per treatment). (Right) Thermal
1051 latency assessed before and after CFA injection with either vehicle (VEH) or SKI II acutely administered on
1052 Day 1; p < 0.0001 (one-way ANOVA; N = 5-7 mice per treatment). Dunnett's test comparisons to baseline
1053 are indicated on graph. Error bars represent mean ± SD. **D.** (Left) 50% withdrawal threshold assessed
1054 before and 24 hours post CFA injection with either vehicle (CFA + VEH) or TY 52156 (CFA + TY) acutely
1055 administered on Day 1; p < 0.0001 (one-way ANOVA; N = 5 mice per treatment). Dunnett's test
1056 comparisons to baseline are indicated on graph. (Right) 50% withdrawal threshold assessed before and

1057 24 hours post CFA injection with either vehicle (CFA + VEH) or SKI II (CFA + SKI II) acutely administered;
1058 *p*-values indicated on graph (two-tailed unpaired t-test; N = 5 mice per group.
1059
1060 **Figure 7-source data 1. S1PR3 is dispensable for development of chronic mechanical**
1061 **hypersensitivity.** *Related to Figure 7.*
1062
1063 **Figure 7-figure supplement 1. S1PR3 KO animals display normal CFA-evoked immune cell**
1064 **recruitment.** *Related to Figure 7.* **A.** Recruitment of neutrophils (Neut.) or inflammatory monocytes (IMs)
1065 to hindpaw skin 24 hours post-CFA administration in S1PR3 HET and KO mice, as a dot plot of CD11b+
1066 cells plotting Ly6G fluorescence intensity vs. Ly6C intensity (AFU). Boxes are for illustrative purposes. **B.**
1067 Recruitment of immune cells, including neutrophils (Neut.) and inflammatory monocytes (IMs) to hindpaw
1068 skin 24 hours post-CFA administration in HET and KO mice, displayed as total number of cells; N = 8 mice
1069 per genotype. Sidak's multiple comparisons were made between HET and KO for each cell type.
1070
1071 **Figure 8. Proposed model illustrating a key role for S1PR3 in regulating mechanical pain in AM**
1072 **nociceptors.** (Top) S1P promotes activation of S1PR3, which leads to inhibition of KCNQ2/3 currents and
1073 promotes normal mechanical pain sensitivity. (Bottom) Diminished S1P or S1PR3 antagonism alleviates
1074 inhibition of KCNQ2/3, leading to mechanical pain hyposensitivity.

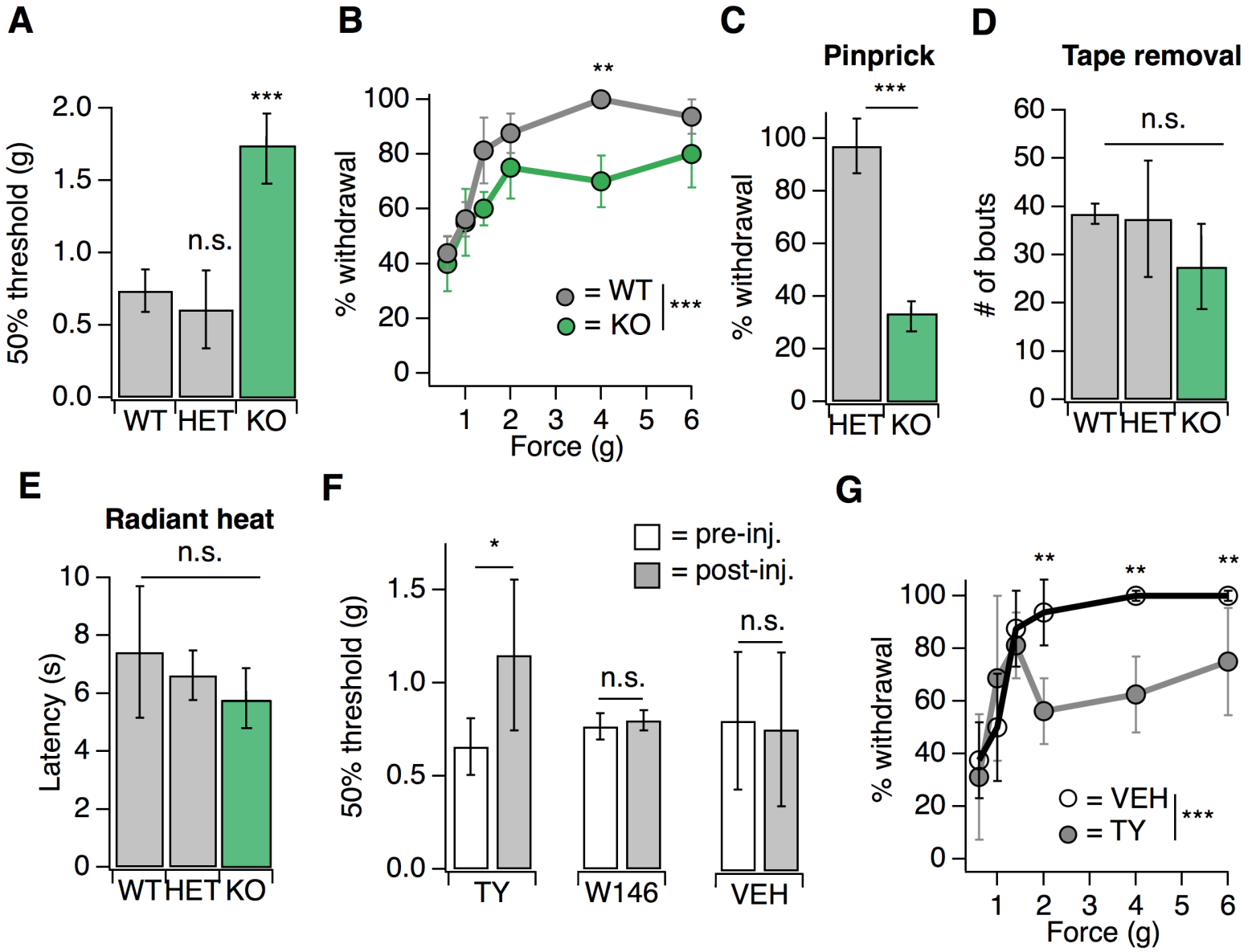
A
50% threshold (g)
2.0
1.5
1.0
0.5
0.0
***
n.s.
WT
HET
KO
B
% withdrawal
100
80
60
40
20
0
**
= WT
= KO
***
1
2
3
4
5
6
Force (g)
C
Pinprick
% withdrawal
100
80
60
40
20
0
***
HET
KO
D
Tape removal
# of bouts
60
50
40
30
20
10
0
n.s.
WT
HET
KO
E
Radiant heat
Latency (s)
10
8
6
4
2
0
n.s.
WT
HET
KO
F
50% threshold (g)
1.5
1.0
0.5
0.0
= pre-inj.
= post-inj.
*
n.s.
n.s.
TY
W146
VEH
G
% withdrawal
100
80
60
40
20
0
**
**
**
= VEH
= TY
***
1
2
3
4
5
6
Force (g)

Figure 1

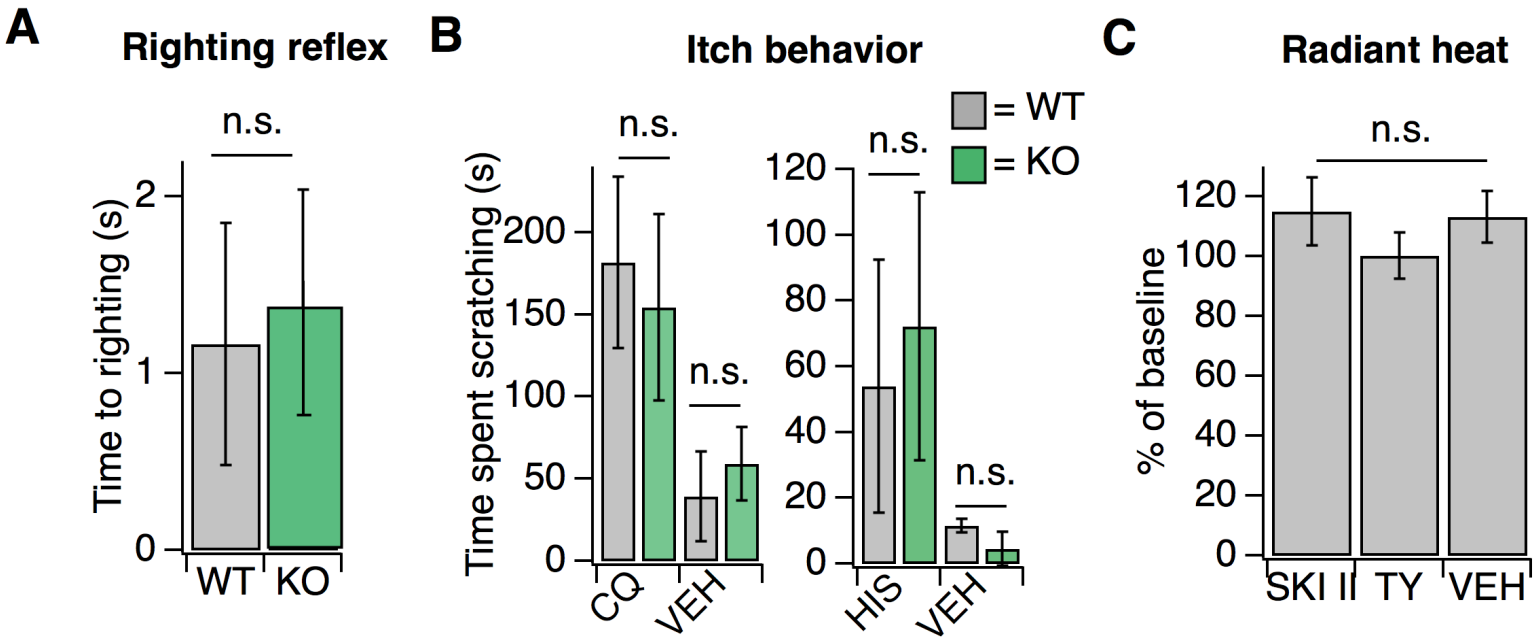

Figure 1-figure supplement 1

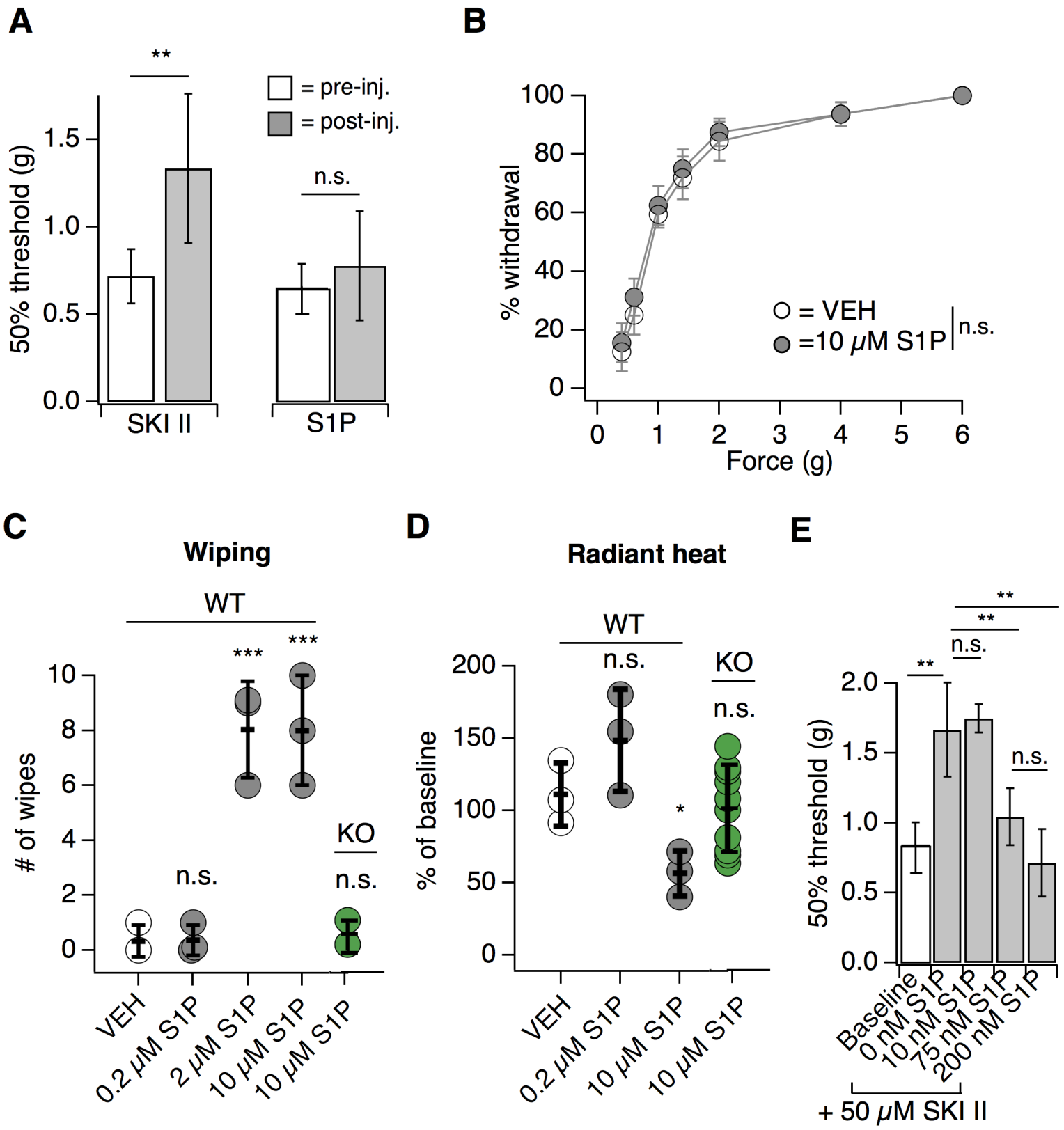
A
**
= pre-inj.
= post-inj.
n.s.
50% threshold (g)
1.5
1.0
0.5
0.0
SKI II
S1P
B
100
80
60
40
20
0
% withdrawal
= VEH
=10 μM S1P
n.s.
0
1
2
3
4
5
6
Force (g)
C
Wiping
WT
***
***
10
8
6
4
2
0
# of wipes
n.s.
KO
n.s.
VEH
0.2 μM S1P
2 μM S1P
10 μM S1P
10 μM S1P
D
Radiant heat
WT
n.s.
KO
n.s.
200
150
100
50
0
% of baseline
*
VEH
0.2 μM S1P
10 μM S1P
10 μM S1P
E
**
**
n.s.
**
n.s.
2.0
1.5
1.0
0.5
0.0
50% threshold (g)
Baseline
0 nM S1P
10 nM S1P
75 nM S1P
200 nM S1P
+ 50 μM SKI II

Figure 2

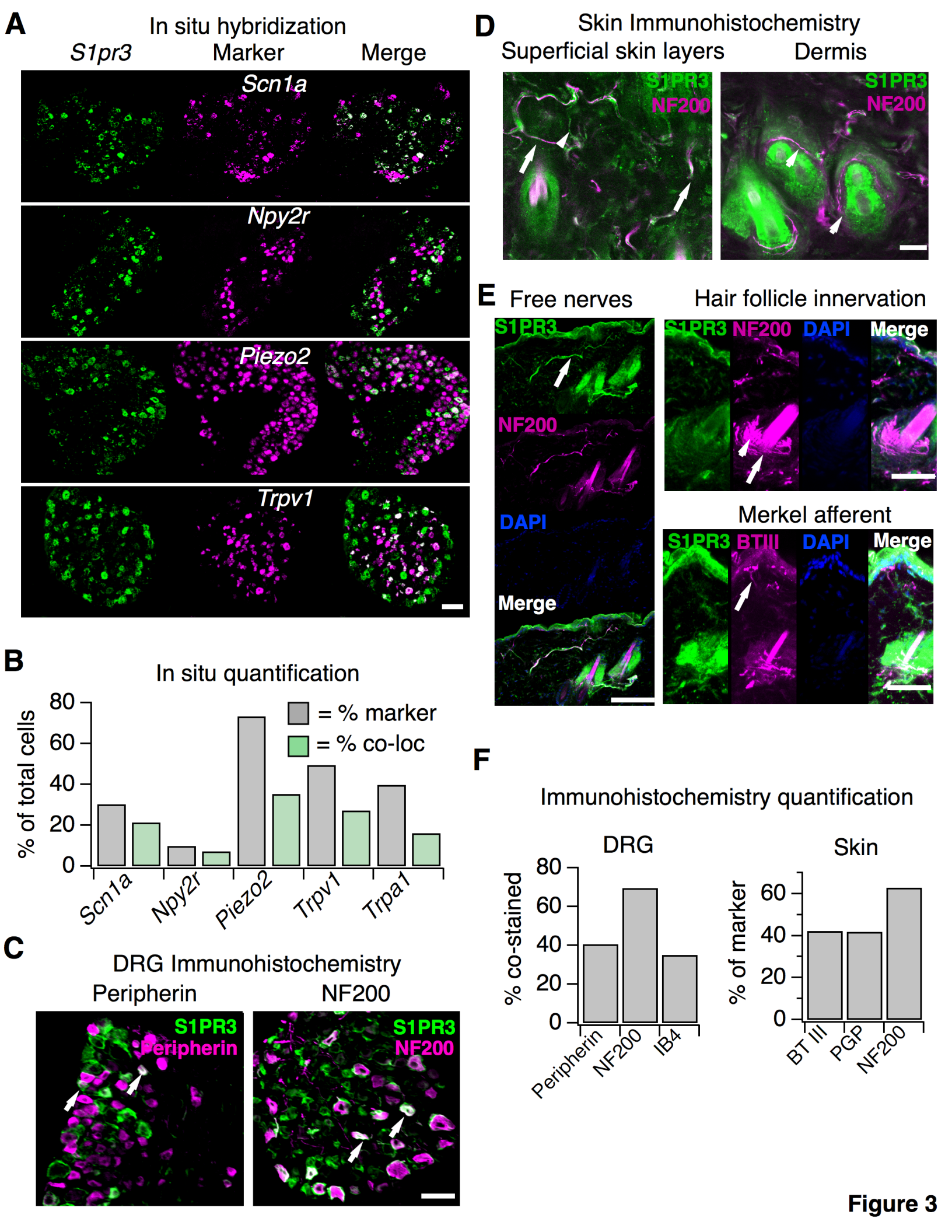
A
In situ hybridization
S1pr3
Marker
Merge
Scn1a
Npy2r
Piezo2
Trpv1
B
In situ quantification
% of total cells
80
60
40
20
0
= % marker
= % co-loc
Scn1a
Npy2r
Piezo2
Trpv1
Trpa1
C
DRG Immunohistochemistry
Peripherin
NF200
S1PR3
Peripherin
S1PR3
NF200
D
Skin Immunohistochemistry
Superficial skin layers
Dermis
S1PR3
NF200
S1PR3
NF200
E
Free nerves
S1PR3
NF200
DAPI
Merge
Hair follicle innervation
S1PR3
NF200
DAPI
Merge
Merkel afferent
S1PR3
BTIII
DAPI
Merge
F
Immunohistochemistry quantification
DRG
% co-stained
80
60
40
20
0
Peripherin
NF200
IB4
Skin
% of marker
60
40
20
0
BT III
PGP
NF200

Figure 3

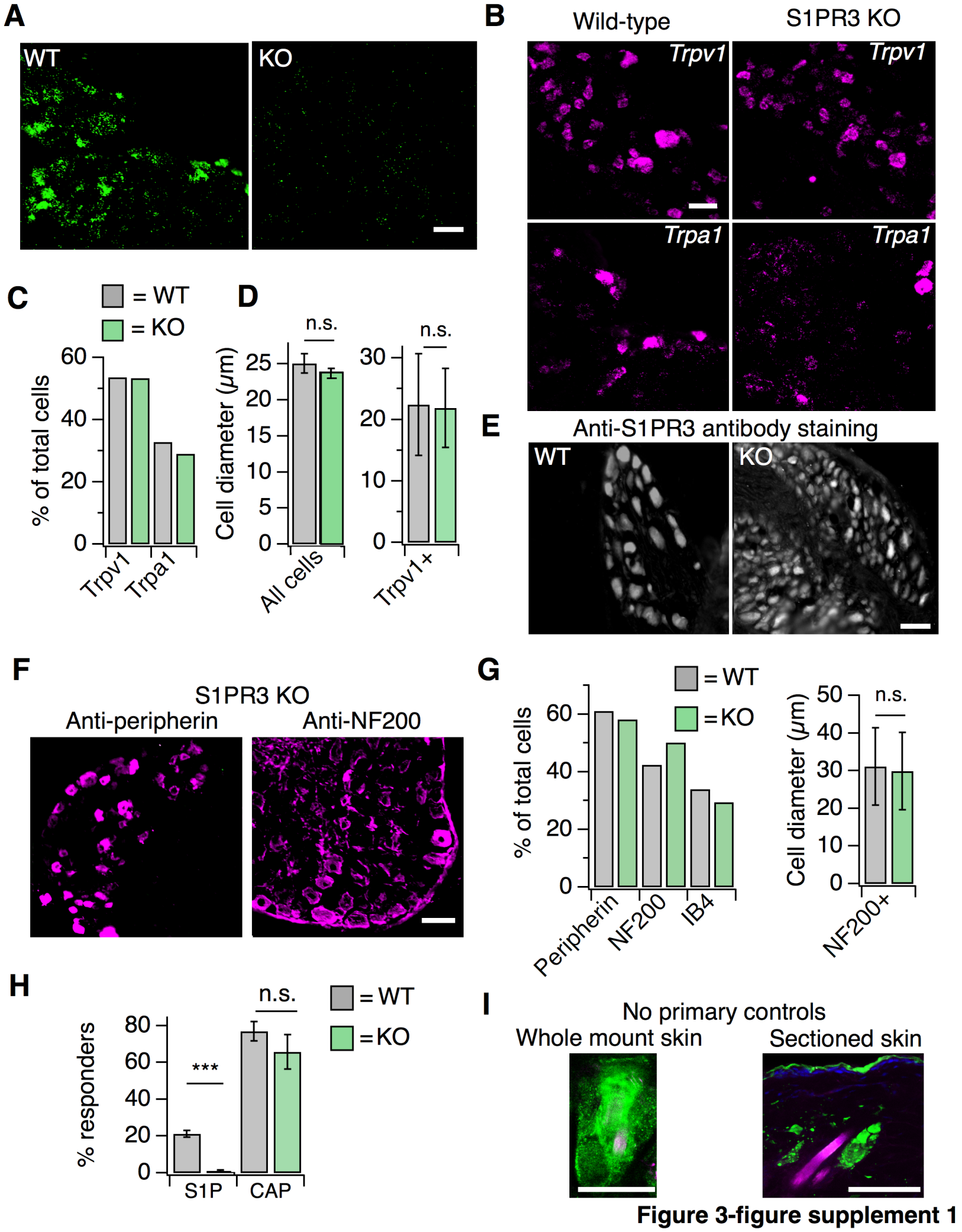

Figure 3-figure supplement 1

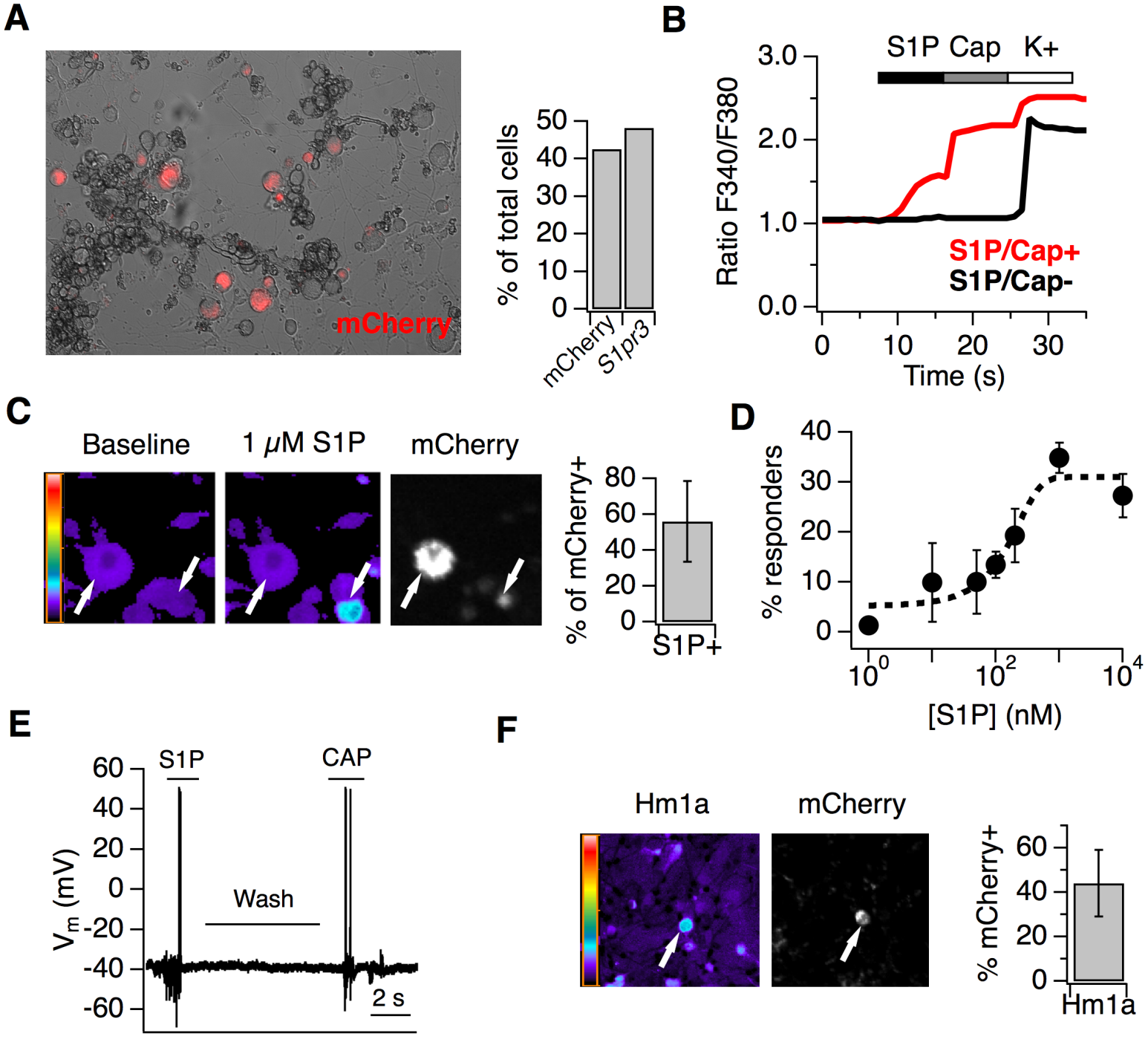
A
mCherry
% of total cells
50
40
30
20
10
0
mCherry
S1pr3
B
S1P Cap K+
Ratio F340/F380
3.0
2.0
1.0
0.0
S1P/Cap+
S1P/Cap-
0
10
20
30
Time (s)
C
Baseline
1 μM S1P
mCherry
% of mCherry+
80
60
40
20
0
S1P+
D
% responders
40
30
20
10
0
10^0
10^2
10^4
[S1P] (nM)
E
S1P
CAP
Wash
Vm (mV)
60
40
20
0
-20
-40
-60
2 s
F
Hm1a
mCherry
% mCherry+
60
40
20
0
Hm1a

Figure 4

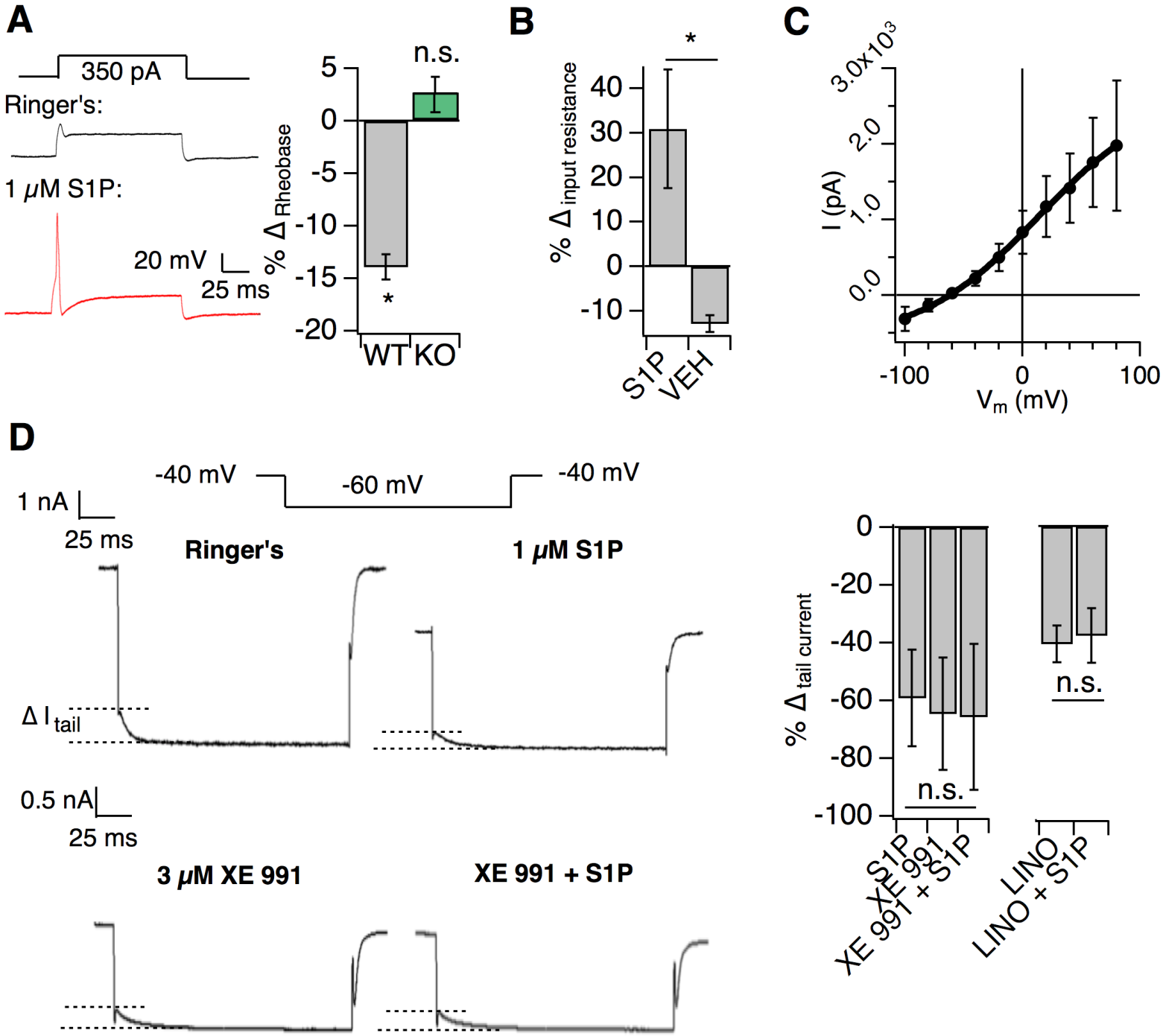
A
350 pA
Ringer's:
1 μM S1P:
20 mV
25 ms
% Δ Rheobase
5
0
-5
-10
-15
-20
n.s.
*
WT
KO
B
% Δ input resistance
40
30
20
10
0
-10
*
S1P
VEH
C
3.0x10³
2.0
1.0
0.0
I (pA)
-100
0
100
Vm (mV)
D
-40 mV
-60 mV
-40 mV
1 nA
25 ms
Ringer's
1 μM S1P
Δ I tail
0.5 nA
25 ms
3 μM XE 991
XE 991 + S1P
% Δ tail current
0
-20
-40
-60
-80
-100
n.s.
n.s.
S1P
XE 991
XE 991 + S1P
LINO
LINO + S1P

Figure 5

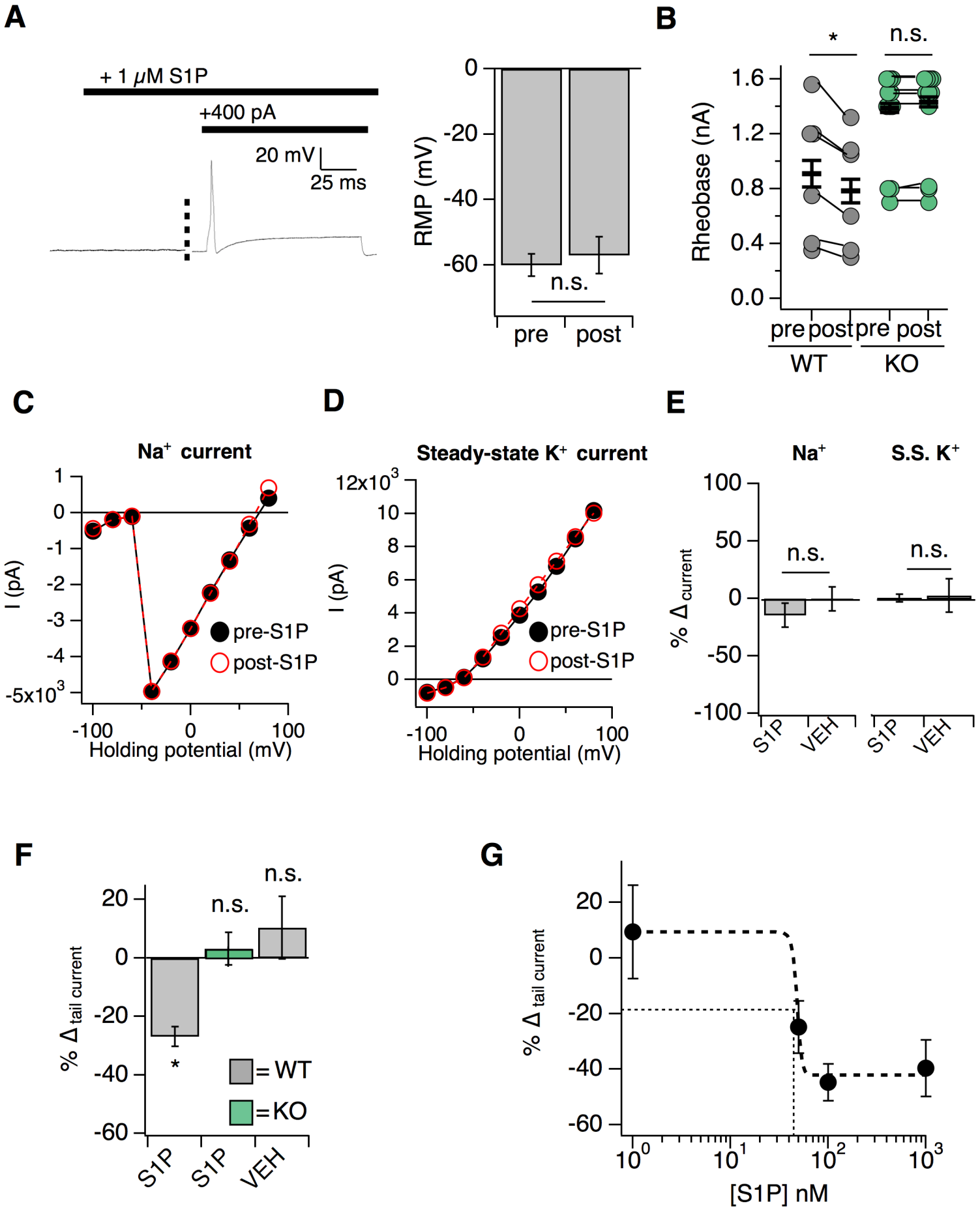

Figure 5-figure supplement 1

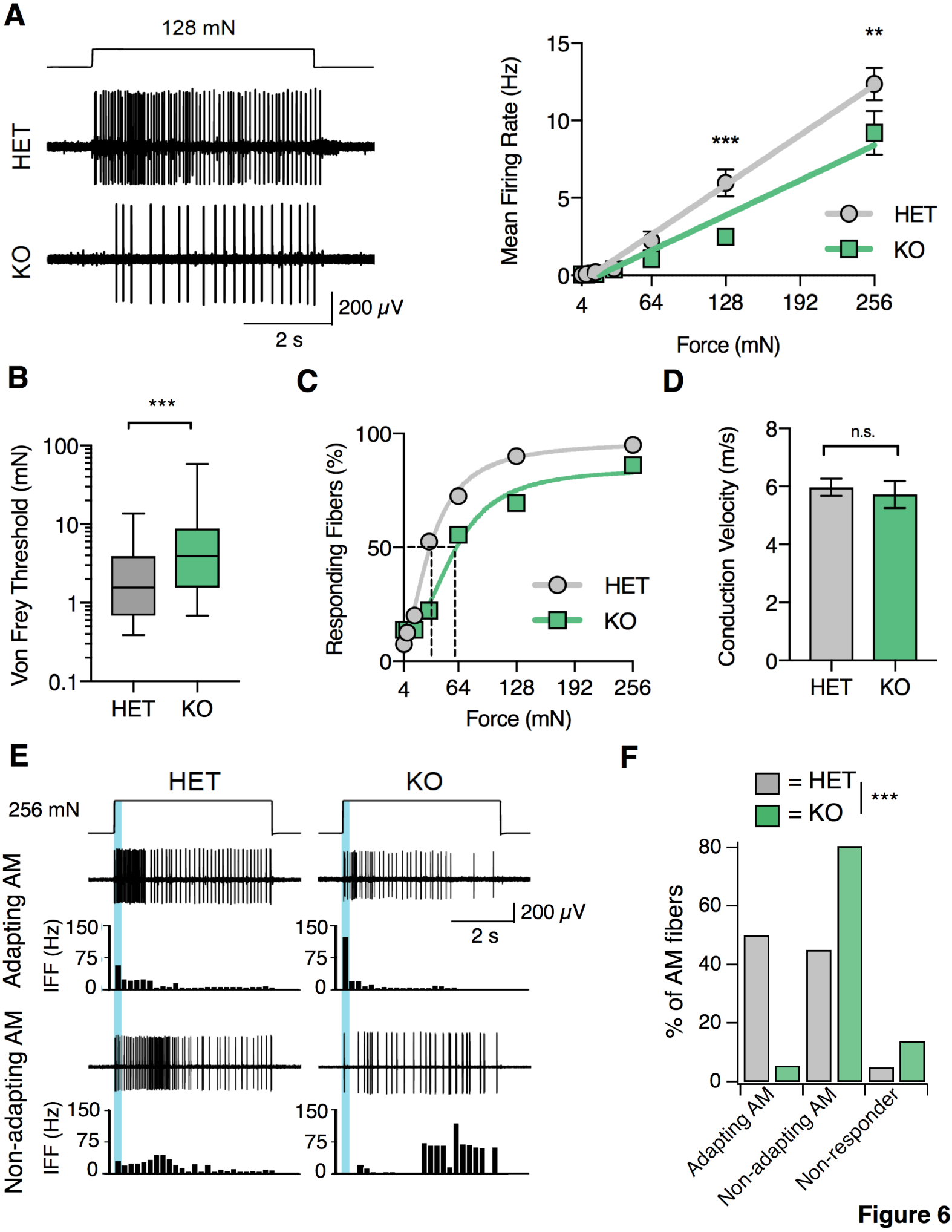
A
128 mN
HET
KO
200 μV
2 s
Mean Firing Rate (Hz)
15
10
5
0
**
***
HET
KO
4
64
128
192
256
Force (mN)
B
***
Von Frey Threshold (mN)
100
10
1
0.1
HET
KO
C
Responding Fibers (%)
100
50
0
HET
KO
4
64
128
192
256
Force (mN)
D
n.s.
Conduction Velocity (m/s)
8
6
4
2
0
HET
KO
E
HET
KO
256 mN
Adapting AM
Non-adapting AM
IFF (Hz)
150
75
0
200 μV
2 s
F
= HET
= KO
***
% of AM fibers
80
60
40
20
0
Adapting AM
Non-adapting AM
Non-responder

Figure 6

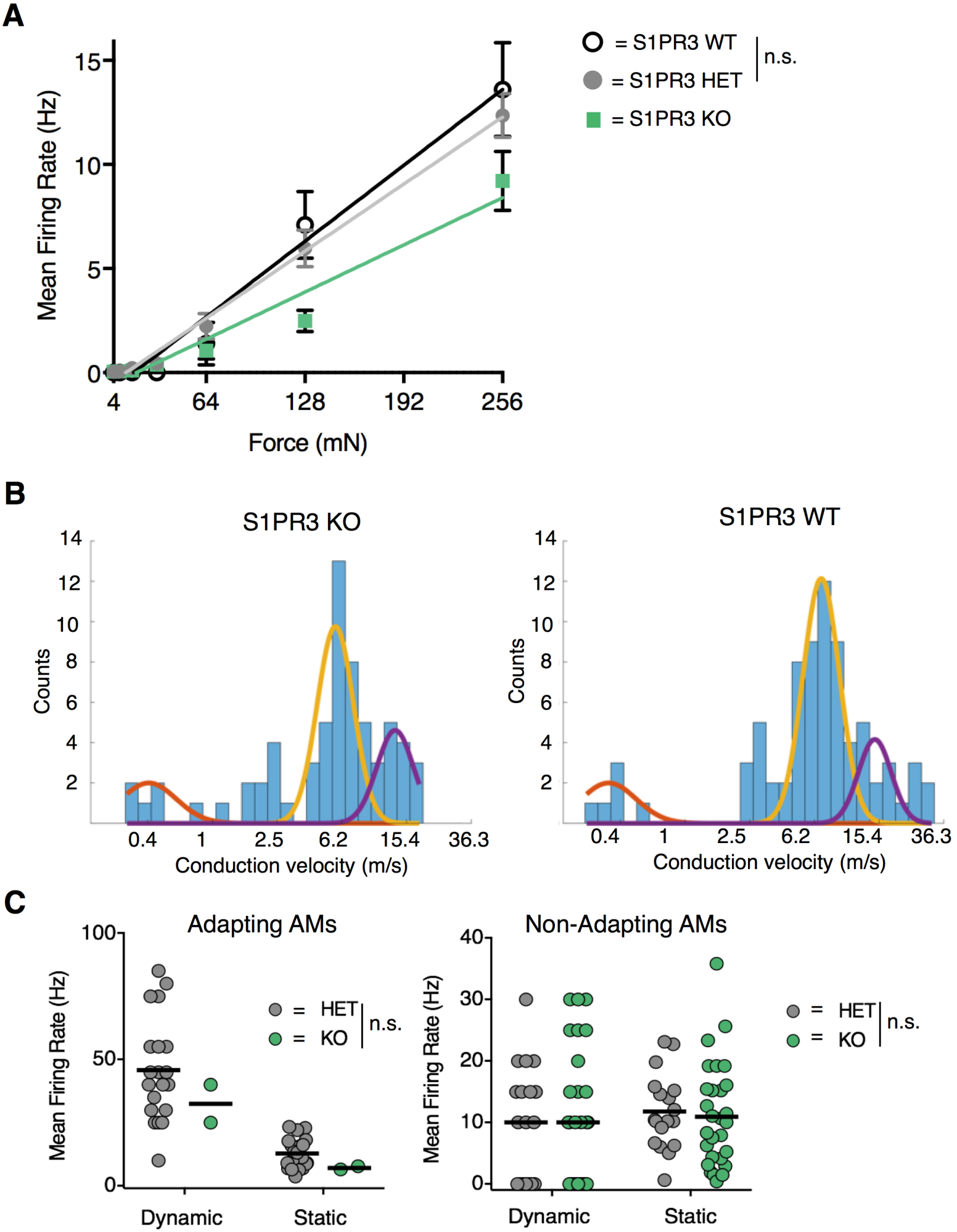

Figure 6-figure supplement 1

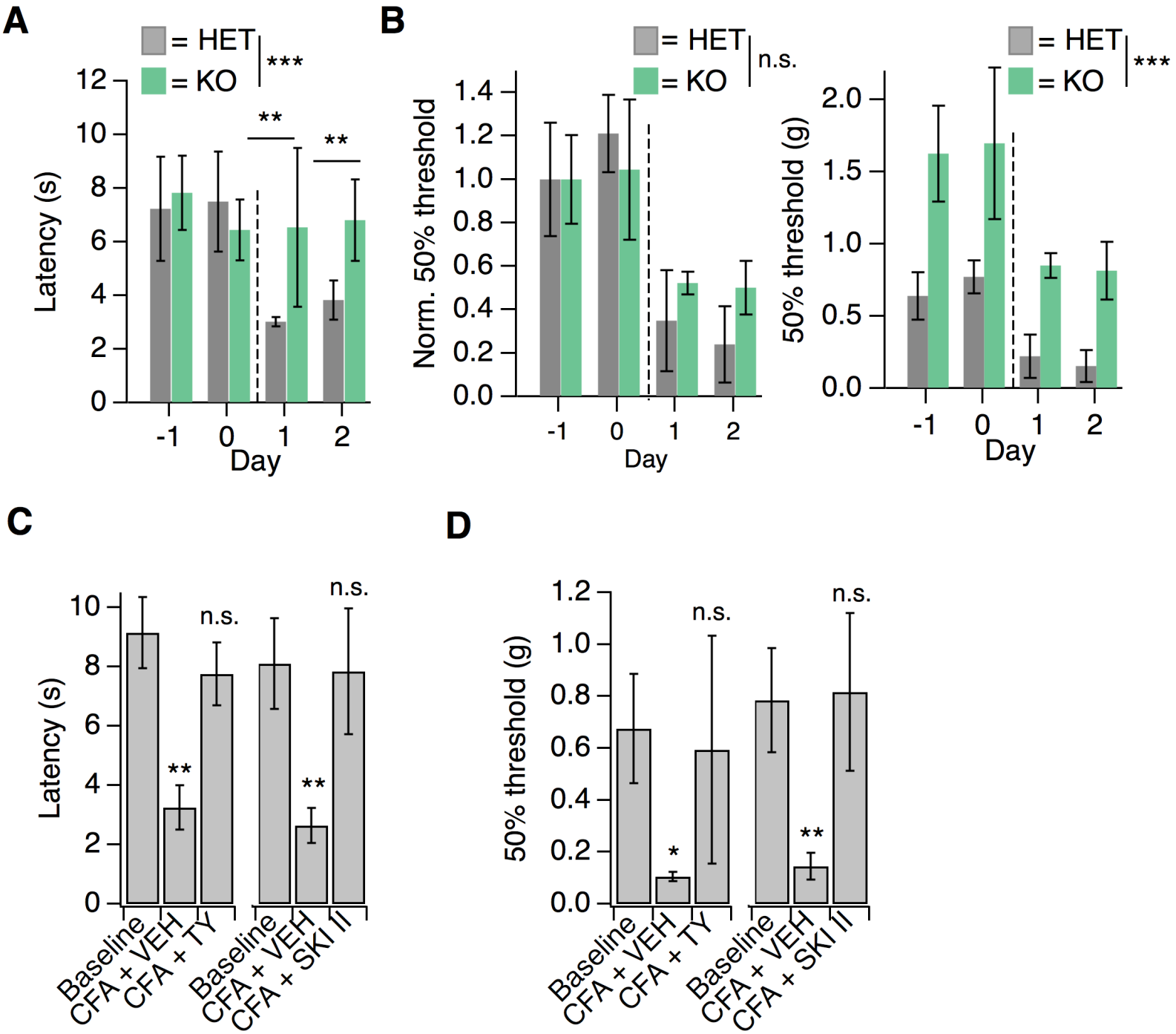
A
= HET
= KO
***
**
**
Latency (s)
Day
B
= HET
= KO
n.s.
Norm. 50% threshold
Day
= HET
= KO
***
50% threshold (g)
Day
C
Latency (s)
n.s.
n.s.
**
**
Baseline
CFA + VEH
CFA + TY
Baseline
CFA + VEH
CFA + SKI II
D
50% threshold (g)
n.s.
n.s.
*
**
Baseline
CFA + VEH
CFA + TY
Baseline
CFA + VEH
CFA + SKI II

Figure 7

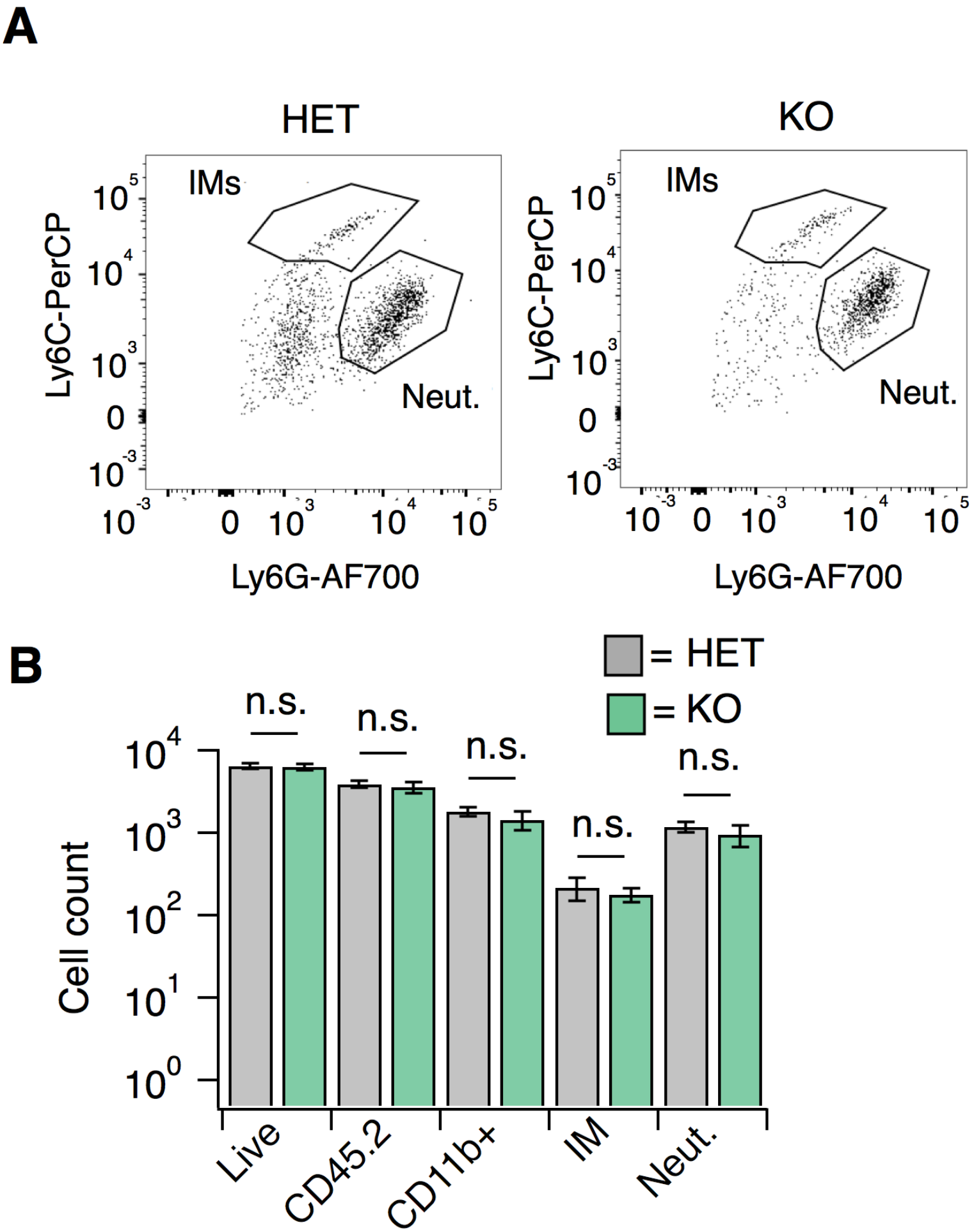

Figure 7-figure supplement 1

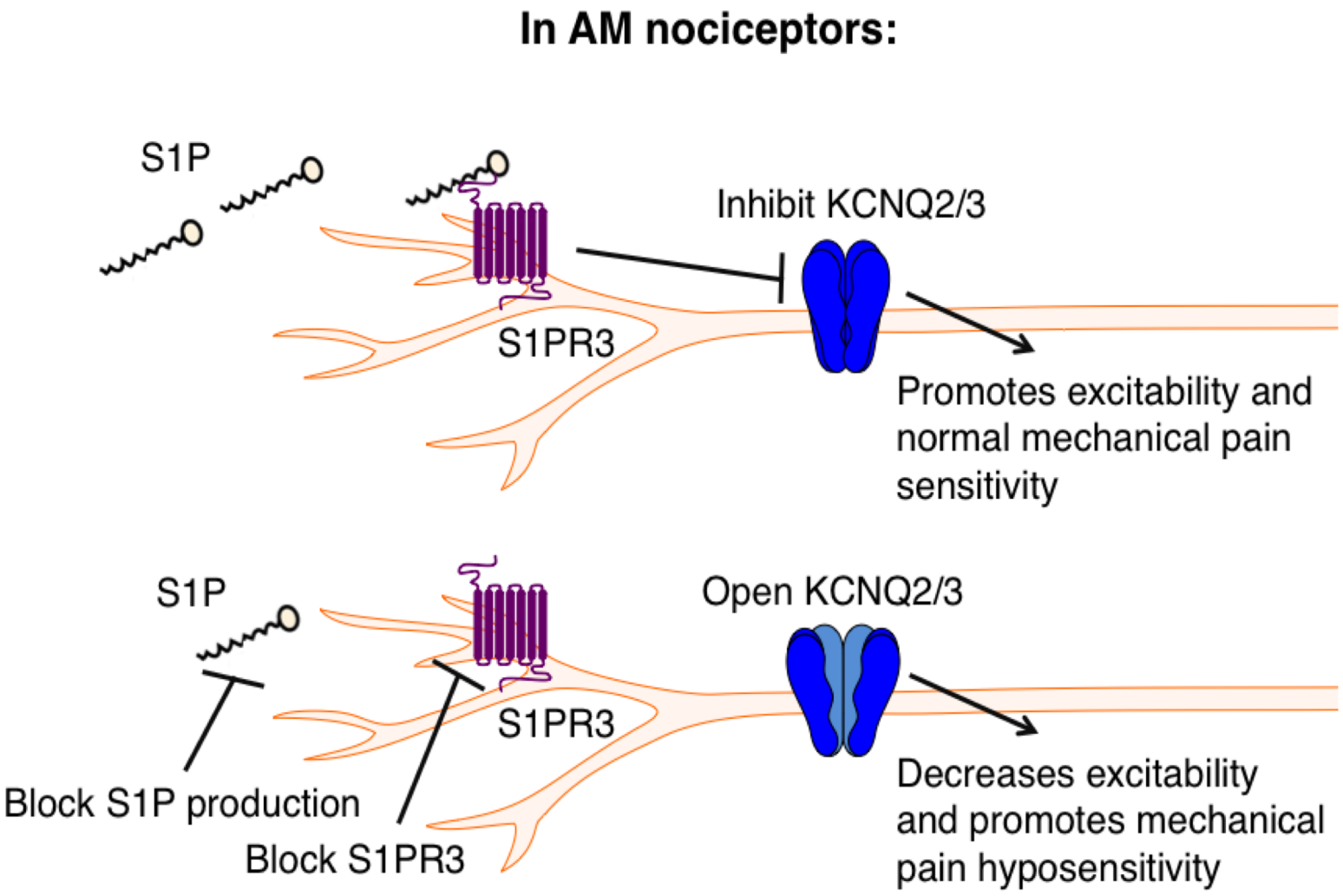
In AM nociceptors:
S1P
Inhibit KCNQ2/3
S1PR3
Promotes excitability and normal mechanical pain sensitivity
S1P
Open KCNQ2/3
S1PR3
Block S1P production
Block S1PR3
Decreases excitability and promotes mechanical pain hyposensitivity

Figure 8